





Article

Design, Synthesis, Molecular Docking, Antiapoptotic and Caspase-3 Inhibition of New 1,2,3-Triazole/Bis-2(1*H*)-Quinolinone Hybrids

Essmat M. El-Sheref ¹, Ashraf A. Aly ^{1,*} , Mohammed B. Alshammari ², Alan B. Brown ³, Sara Mohamed Naguib Abdel-Hafez ⁴, Walaa Yehia Abdelzaher ⁵ , Stefan Bräse ^{6,7,*}  and ElShimaa M. N. Abdelhafez ⁸ 

¹ Chemistry Department, Faculty of Science, Minia University, El-Minia 61519, Egypt; e.m.elsheref1980@gmail.com

² College of Sciences and Humanities, Prince Sattam bin Abdulaziz University, Alkharj 11942, Saudi Arabia; m.alshammari@psau.edu.sa

³ Florida Institute of Technology, 150 W University Blvd, Melbourne, FL 32901, USA; abrown@fit.edu

⁴ Faculty of Medicine, Histology Department, Minia University, El-Minia 61519, Egypt; sara_histology@yahoo.com

⁵ Faculty of Medicine, Pharmacology Department, Minia University, El-Minia 61519, Egypt; walaayehia22@yahoo.com

⁶ Institute of Organic Chemistry, Karlsruhe Institute of Technology, 76131 Karlsruhe, Germany

⁷ Institute of Biological and Chemical Systems (IBCS-FMS), Karlsruhe Institute of Technology, 76344 Eggenstein-Leopoldshafen, Germany

⁸ Department of Medicinal Chemistry, Faculty of Pharmacy, Minia University, El-Minia 61519, Egypt; shimaanaguib_80@yahoo.com

* Correspondence: ashrafaly63@yahoo.com or ashraf.shehata@mu.edu.eg (A.A.A.); braese@kit.edu (S.B.); Tel.: +20-1006268742 (A.A.A.); +49-721-608-42902 (S.B.)

Received: 1 October 2020; Accepted: 22 October 2020; Published: 30 October 2020



Abstract: A series of novel 1,2,3-triazoles hybridized with two quinolin-2-ones, was designed and synthesized through click reactions. The structures of the synthesized compounds were elucidated by NMR, IR, and mass spectra in addition to elemental analysis. The synthesized compounds were assessed for their antiapoptotic activity in testis, as testicular torsion is the main cause of male infertility. This effect was studied in light of decreasing tissue damage induced by I/R in the testis of rats using *N*-acetylcysteine (NAC) as an antiapoptotic reference. Compounds **6a–c** were the most active antiapoptotic hybrids with significant measurements for malondialdehyde (MDA) and total antioxidant capacity (TAC) and the apoptotic biomarkers (testicular testosterone, TNF α , and caspase-3) in comparison to the reference. A preliminary mechanistic study was performed to improve the antiapoptotic activity through caspase-3 inhibition. A compound assigned as 6-methoxy-4-(4-(((2-oxo-1,2-dihydroquinolin-4-yl)oxy)methyl)-1*H*-1,2,3-triazol-1-yl)quinolin-2(1*H*)-one (**6c**) was selected as a representative of the most active hybrids in comparison to NAC. Assay of cytochrome C for **6c** revealed an attenuation of cytochrome C level about 3.54 fold, comparable to NAC (4.13 fold). In caspases-3,8,9 assays, **6c** was found to exhibit more potency and selectivity toward caspase-3 than other caspases. The testicular histopathological investigation was carried out on all targeted compounds **6a–g**, indicating a significant improvement in the spermatogenesis process for compounds **6a–c** if compared to the reference relative to the control. Finally, molecular docking studies were done at the caspase-3 active site to suggest possible binding modes. Hence, it could conceivably be hypothesized that compounds **6a–c** could be considered good lead candidate compounds as antiapoptotic agents.

Keywords: caspase-3; 1,2,3-triazole-biquinolin-2-one; antiapoptotic; NAC; histopathology; antioxidant; testis; docking

1. Introduction

Apoptosis is an essential programmed biological process in cells during animal development, [1] homeostasis [2], and immune responses [3]. Although apoptosis occurs normally in tissues, imbalance probably occurs in some cases between apoptotic and antiapoptotic mediators leading to some diseases [4]. Apoptosis could be abrogated, which means cells that should be eliminated may persist and become immortal, for example, in cancer [5] and autoimmunity [6]. On the other hand, when apoptosis exaggerated, it kills too many cells and inflicts grave tissue damage; as in strokes [7], neurodegenerative disorders such as Alzheimer's [8], retinal cell death [9], myocardial and testicular ischemia [10,11] inflammatory diseases such as rheumatoid arthritis [12], sepsis [13], osteoarthritis (OA) [14], and asthma [15].

The caspase family has been an intensely studied target in drug design for many years [1]. To date, 14 mammalian caspases were identified, among them, caspase -2, -3, -6, -7, -8, -9, and -10, which were described as apoptotic caspases [1]. Interestingly, caspase-3 was found to be generally more promiscuous than caspase-7, 8, and 9 and revealed the major executioner caspase during the demolition phase of apoptosis [16,17]. Additionally, caspase-3 plays a key executioner role and its inhibition can drastically prevent apoptosis in vitro and in vivo [1].

Currently, one of the urological emergency conditions in male infertility is testicular torsion, which is common in new-born kids, children, and adolescent boys [18,19]. Testicular torsion, or a twisted spermatic cord, decreases the blood flow to the testis, causing tissue ischemia and a loss of germ cells [20]. Previous studies have shown that the pathophysiology of testicular torsion/detorsion centers around acute ischemia/reperfusion (I/R) injury of the testis resulting in the possibility of infertility whereas torsion comprises the ischemic period, while detorsion comprises reperfusion injury [21]. Therefore, several studies have been revealed that testicular torsion/detorsion or (I/R) injury triggers the generation of reactive oxygen species, proinflammatory cytokines, anoxia, and apoptosis, which is followed by activation of the necrosis/apoptosis pathway, possibly causing subsequent infertility [22].

On the other hand, the discovery of quinolone-based drugs has attracted wide attention due to their diverse spectrum of biological activities [23] as an antimicrobial effect [24,25]. Arylidenes of the quinolin-2-one scaffold with anticancer activity was working as Erlotinib analogs with activities against leukemia through inhibition of EGFR TK/STAT-3 pathways [26], however, other quinoline-2-one/pyrazole derivatives exhibited antiapoptotic activity with caspase-3 inhibition [1].

The promising application of triazoles in drug design such as anti-tuberculosis [27], anticancer [28], and the lead compound, SN606078, 2-(2,6-dichloro-4-trifluoromethylphenyl)-4-(4,5-dicyano-1H-imidazol-2-yl)-2H-1,2,3-triazole acting as antagonists of GABA receptors [29,30] is further propelled by the advent of click chemistry in the synthesis of triazoles [31].

Recently, there have been several reports of potential therapeutic agents comprising either quinoline or triazole scaffold each in a discrete molecule, which were investigated against (I/R) injury through apoptosis inhibition. In 2003, Kojima et al. [32] reported on Rebamipide I as an antioxidative agent able to attenuate the elevation in apoptosis in the intestinal mucosa after I/R through caspase-3 inhibition, but not to completely abolish it [32]. This can be seen also in the case of compound II, a quinoline containing scaffold that exhibited antiapoptotic activity through inhibition of caspase-3 with an $IC_{50} = 4$ nM (Figure 1) [1].

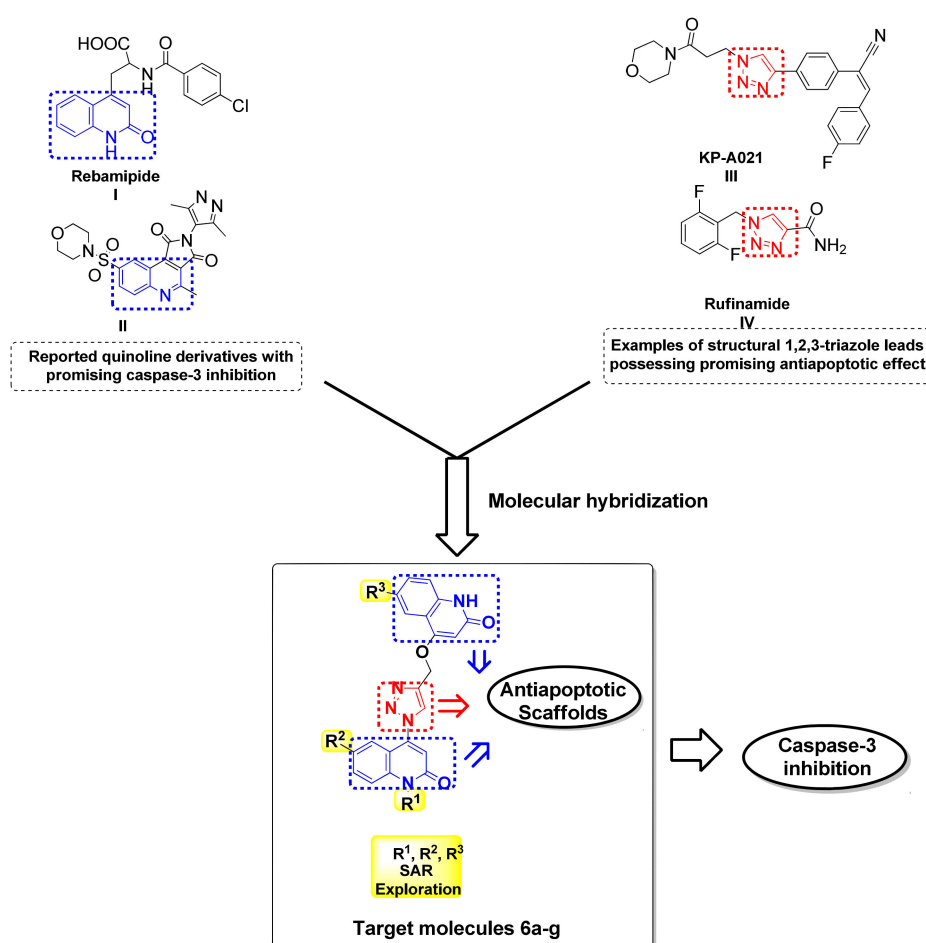


Figure 1. Examples of reported quinoline and 1,2,3-triazole based antiapoptotic drugs and caspase-3 and the design strategy for the target hybrids 6a-g.

Additionally, the 1,2,3-triazole-based scaffold was reported for KPRA020 **III** to be used as an antioxidant and antiapoptotic agent to prevent ototoxicity caused by cisplatin-induced oxidative stress [33]. Furthermore, the results demonstrated by Park et al. suggested that Rufinamide **V** can display a neuroprotective effect against cerebral ischemia involving the attenuation of ischemia-induced glial activation [34] (Figure 1).

In response to the previously mentioned aspects, we here reported our medicinal chemistry efforts, starting from the core scaffold of caspase inhibitor that led to gathering two types of scaffolds, triazole and quinolin-2-one, respectively, in one compact hybrid to design simpler and more efficient antiapoptotic compounds investigating the caspase-3 inhibition to minimize, or even prevent, testicular I/R injury as illustrated in a summarized schematic diagram (Figure 2).

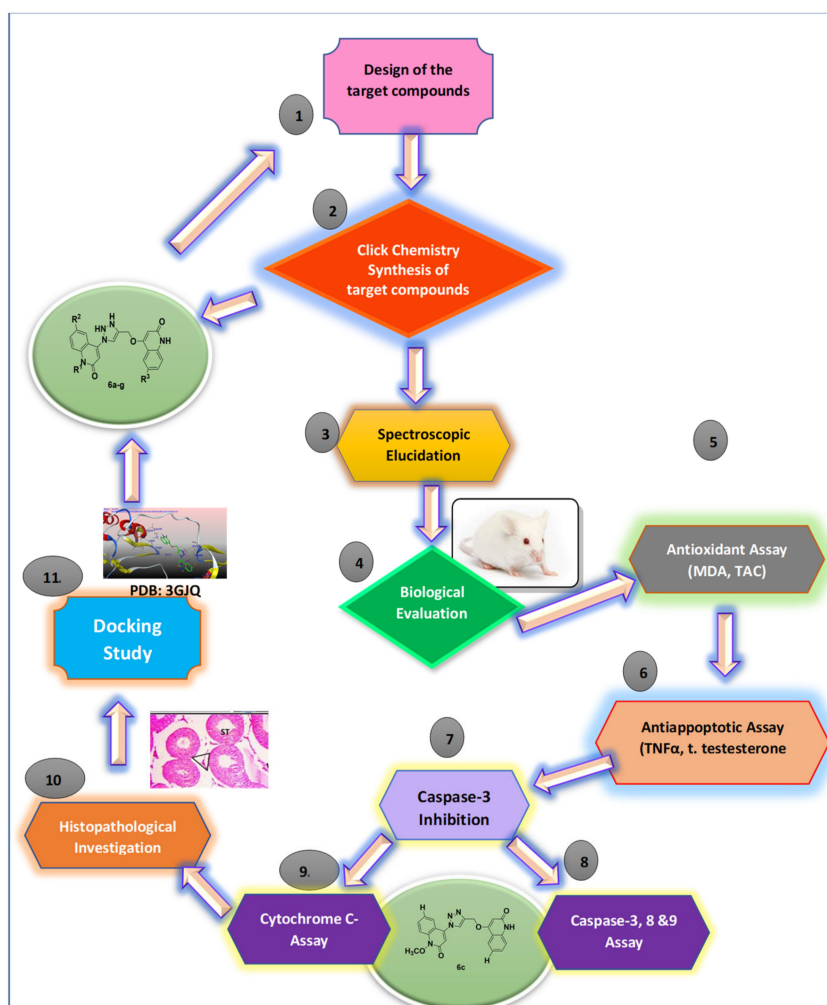


Figure 2. Schematic diagram illustrating all methodological steps.

2. Results and Discussion

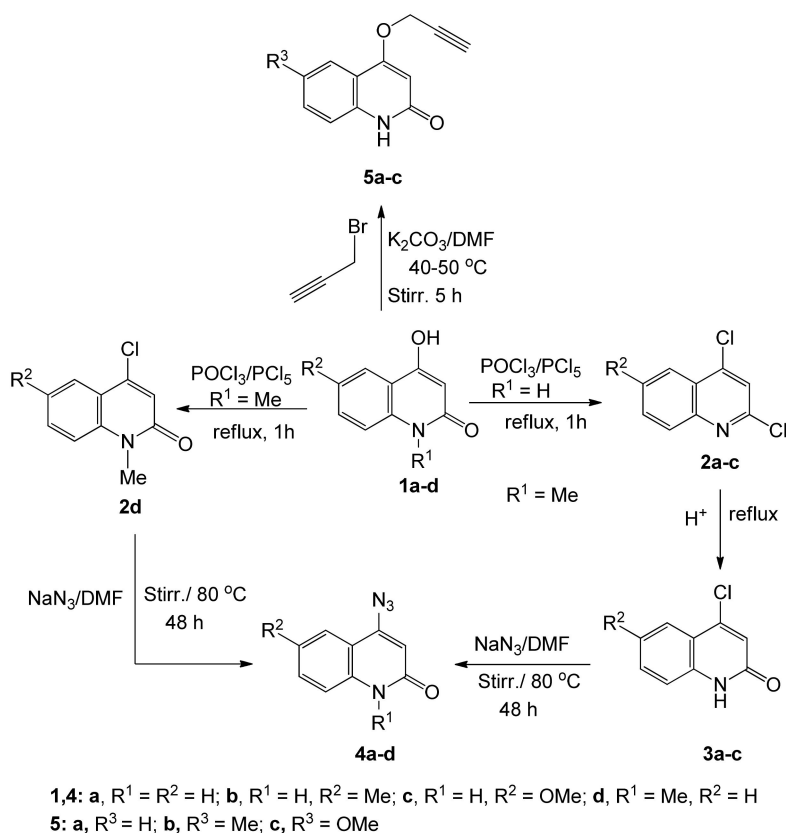
2.1. Chemistry

To obtain 4-azidoquinolin-2(1*H*)-ones **4a–d**, 4-hydroxy-2-quinolinones **1a–d** were synthesized according to literature procedures [35,36], then treated with excess POCl₃ in the presence of PCI₅ at reflux for 1 h to give 2,4-dichloroquinolines **2a–c** and 4-chloro-2-quinolinone **2d** [37].

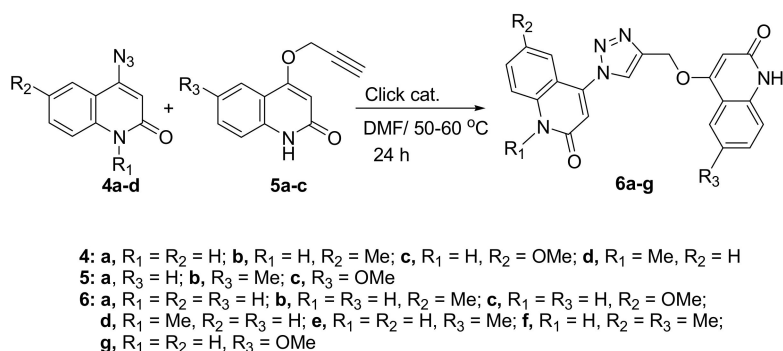
Compounds **2a–c** were heated with acetic acid/water (3:1) at reflux, to convert the Cl-group in position 2 into a carbonyl group to obtain 4-chloro-2-quinolinones **3a–c** [38]. Finally, either **2d** or **3a–c** was subjected to sodium azide in DMF with stirring at 70–80 °C, to give 4-azidoquinolin-2(1*H*)-ones **4a–d** according to literature procedures [38–41] (Scheme 1). The reaction of 6-substituted 4-hydroxy-quinolin-2(1*H*)-ones **1a–d** in DMF and K₂CO₃ with propargyl bromide gave products **5a–c** as white precipitates (Scheme 1).

Aly et al. reported on the promising aspect of 3,3'-methylenebis(4-hydroxyquinolin-2(1*H*)-ones) as anti-Covid-19 [42]. In our present work, 1,2,3-triazoles were accessed by Huisgen type thermal 1,3-dipolar addition, which resulted in a mixture of 1,4- and 1,5-disubstituted triazoles [43]. The novel hybrids **6a–g** were synthesized through click chemistry, which is a powerful tool for quick, highly selective, and reliable access to a reaction product with good yields. Therefore, we carried out the [3+2] cycloadditions of 4-azidoquinolin-2(1*H*)-ones **4a–d** with 4-(prop-2-yn-1-yloxy)quinolin

-2(1*H*)-ones **5a–c** to give the corresponding 4-((1-(2-oxo-1,2-dihydroquinolin-4-yl)-1*H*-1,2,3-triazol-4-yl)methoxy)quinolin-2(1*H*)-ones **6a–g** (Scheme 2).



Scheme 1. Preparation of starting materials **4a–d** and **5a–c**.



Scheme 2. Click reactions between 4-azidoquinolin-2(1*H*)-ones **4a–d** and alkynes **5a–c**.

In the published synthesis of 4-(prop-2-yn-1-yloxy)quinolin-2(1*H*)-one (**5a**) [44], it is described as a quinolin-2-ol **8** (Figure 3). However, we observe an HSQC correlation between *N*-1 and *H*-1 not only for **5a** but throughout series **5** and **6** (Table 1). The HSQC sequence with standard settings (in this case, $^1J_{N-H} = 90$ Hz) is well-known to detect one-bond N-H couplings but not long-range couplings [33,34]; therefore, we assign the series **4–6** as quinolin-2(1*H*)-ones. Our chemical shifts for **5a** in CDCl₃ do not match those reported for **8** [32]; the tautomer population may vary with different samples.

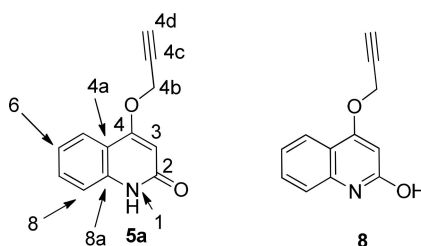


Figure 3. Structure of 4-(prop-2-yn-1-yloxy)quinolin-2(1H)-one: **5a** rather than **8**.

Table 1. ^1H - ^{15}N HSQC correlations in Series 5 and 6.

Compound	δ_{H} (H-1)	δ_{N} (N-1)	Solvent
5a	144.1	11.44	DMSO- d_6
	145.3	11.95	CDCl_3
5b	144.1	11.37	DMSO- d_6
5c	144.1	11.36	DMSO- d_6
6b	144.0 (N-1')	11.43 (H-1')	DMSO- d_6
	151.6	12.29	
6d	144.1 (N-1')	11.43 (H-1')	DMSO- d_6
6e	143.2 (N-1')	11.35 (H-1')	DMSO- d_6
	152.2	12.29	
6f	143.2 (N-1')	11.36 (H-1')	DMSO- d_6
	151.5	12.22	

(Compounds not shown were too insoluble for H-N correlation experiments).

The structures of compounds **6a–g** were confirmed by using different spectral data such as ^1H -NMR, ^{13}C -NMR, 2D-NMR, ^{15}N -NMR, and mass spectrometry, as well as elemental analyses. For example, compound **6b** was assigned as 6-methyl-4-(4-(((2-oxo-1,2-dihydroquinolin-4-yl)oxy)methyl)-1H-1,2,3-triazol-1-yl)quinolin-2(1H)-one. It exhibited a molecular formula of $\text{C}_{22}\text{H}_{17}\text{N}_5\text{O}_3$, representing a product from one molecule of **4b** and one molecule of **5a** without elimination. This result was further confirmed by mass spectrometry with $m/z = 399$ and elemental analysis (Figure 4). In the ^1H -NMR spectrum of compound **6b**, two quinolinone-NH protons appeared as broad signals at δ_{H} 12.22 and 11.44, one of them for the quinolinone carrying the triazole ring and the other one for the quinolinone initially carrying the propargyloxy group, respectively; these two protons were assigned exactly by analogy with compound **7** (Figure 4) [35] and from 2D-NMR (Table 2). Also, there were two doublets at δ_{H} 7.84 ($J = 6.8$ Hz; H-5') and 7.30 ($J = 7.4$ Hz; H-8'), and five singlets at δ_{H} 8.98, 6.86, 6.22, 5.48 and 2.31, which were assigned as H-5'', H-3, H-3', CH_2 and CH_3 , respectively.

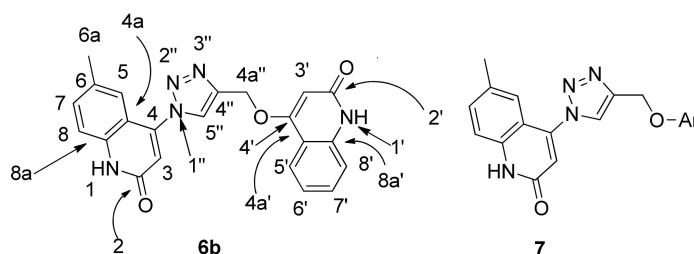


Figure 4. 6-methyl-4-(4-(((2-oxo-1,2-dihydroquinolin-4-yl)oxy)methyl)-1H-1,2,3-triazol-1-yl)quinolin-2(1H)-one **6b** and **7** (Ar = *p*-formylphenyl).

Table 2. NMR data for compound 6b.

¹ H-NMR (DMSO- <i>d</i> ₆)	¹ H- ¹ H COSY		Assig.
12.22 (bs; 1H)			H-1
11.44 (bs; 1H)			H-1'
8.98 (s; 1H)			H-5''
7.84 (d, <i>J</i> = 6.8; 1H)	7.15		H-5'
7.51-7.49 (m; 2H)	7.40, 7.30, 7.15		H-7,7'
7.40 (m; 1H)	7.50		H-8
7.30 (d, <i>J</i> = 7.4; 1H)	7.50		H-8'
7.27 (bs; 1H)	2.31		H-5
7.15 (m; 1H)	7.84, 7.51		H-6'
6.86 (s; 1H)			H-3
6.22 (s; 1H)			H-3'
5.48 (s; 2H)			H-4a''
2.31 (s; 3H)	7.27		H-6a
¹³ C-NMR (DMSO- <i>d</i> ₆)	HSQC	HMBC	Assig.
163.16			C-2'
161.27		7.84, 6.22, 5.48	C-4'
160.83			C-2
143.38		7.27, 6.86	C-4
142.39		8.98, 5.47	C-4''
138.66		7.84, 7.51	C-8a'
137.52		7.49, 7.27	C-4
133.18	7.49	2.31	C-7
131.79			C-6
131.02	7.51	7.84	C-7'
126.73	8.98	5.48	C-5''
123.17	7.27	2.31	C-5
122.49	7.84	7.29	C-5'
121.32	7.15	7.30	C-6'
117.81	6.86		C-3
115.92			C-4a/4a'
115.16	7.40	7.27, 6.91	C-8
114.42	7.30	7.15, 6.22	C-8', 4a'/4a
97.93	6.22		C-3'
61.81	5.48		C-4a''
20.52	2.31	2.31	C-6a
¹⁵ N-NMR (DMSO- <i>d</i> ₆)	HSQC	HMBC	Assig.
248.0		8.98	N-1''
151.6	12.29		N-1
144.0	11.43		N-1'

In the ¹³C-NMR spectrum of **6b**, two signals appeared at δ_C 163.16 and 160.83, for two carbonyl groups assigned as C-2' and C-2, respectively. Also, the signal at δ_C 61.81, which gives HSQC correlation with the proton at δ_H 5.48, was assigned as C-4a'' (methylene group). The signal at δ_C 20.52 ppm, which gives HSQC and HMBC correlation with the proton signal at δ_H 2.31, and H–H correlation with the proton at δ_H 7.27, was assigned as C-6a (methyl group). Other signals in the ¹³C-NMR of **6b** appeared at δ_C 161.75, 143.38, 126.73, 123.81, 117.81 and 97.93, and were assigned to C-4', C-4'', C-5'', C-5, C-3 and C-3', respectively (Table 2). Also, the triazole signals were distinctive in the proton spectrum at δ_H 5.48 (2H; H-4a'') and 8.98 (1H; H-5''); correlations with the proton signals led to the assignment of the carbons at δ_C 142.39 (C-4''), 126.73 (C-5''), and 61.81 (C-4a''). ¹⁵N-NMR showed three types of nitrogen. One appears at δ_N 248.0, which indicates an *sp*² nitrogen; it was assigned as N-1'' and gives HMBC correlation with a proton at δ_H 8.98 (H-5'') but gives no HSQC correlation. The other two nitrogen atoms resonated at δ_N 151.6 and 144.0; their chemical shifts are characteristic of

amide-type nitrogen atoms, and they give HSQC correlation with the attached protons at δ_H 12.29 and 11.43; therefore, these nitrogen atoms were assigned as N-1 and N-1', respectively.

2.2. Evaluation of Biological Activity

This section describes the methods used in the investigation of the antiapoptotic effect of the novel compounds **6a–g** then supported by further histological and molecular docking studies. The antiapoptotic effect of **6a–g** was evaluated through evaluation of decreasing tissue damage induced by I/R in the testis of rats in a dose equivalent to 30 mg *N*-acetylcysteine (NAC) as an antiapoptotic reference [45,46]. The rats were subdivided into sham, I/R, NAC and treated with tested compounds groups, each group comprises of 6 rats (weighing 140–150 g). The targeted compounds **6a–g** were administrated intra-peritoneal (i.p.) an hour before ischemia, which lasted for (0.5 h) then reperfusion (1 h) followed by cutting the organ (Figure 5). Different biomarkers concentrations were measured in serum to detect testis injury due to ischemia/reperfusion (I/R). Some of these biomarkers are increased and others decreased indicating an apoptotic effect as shown in Table 3.

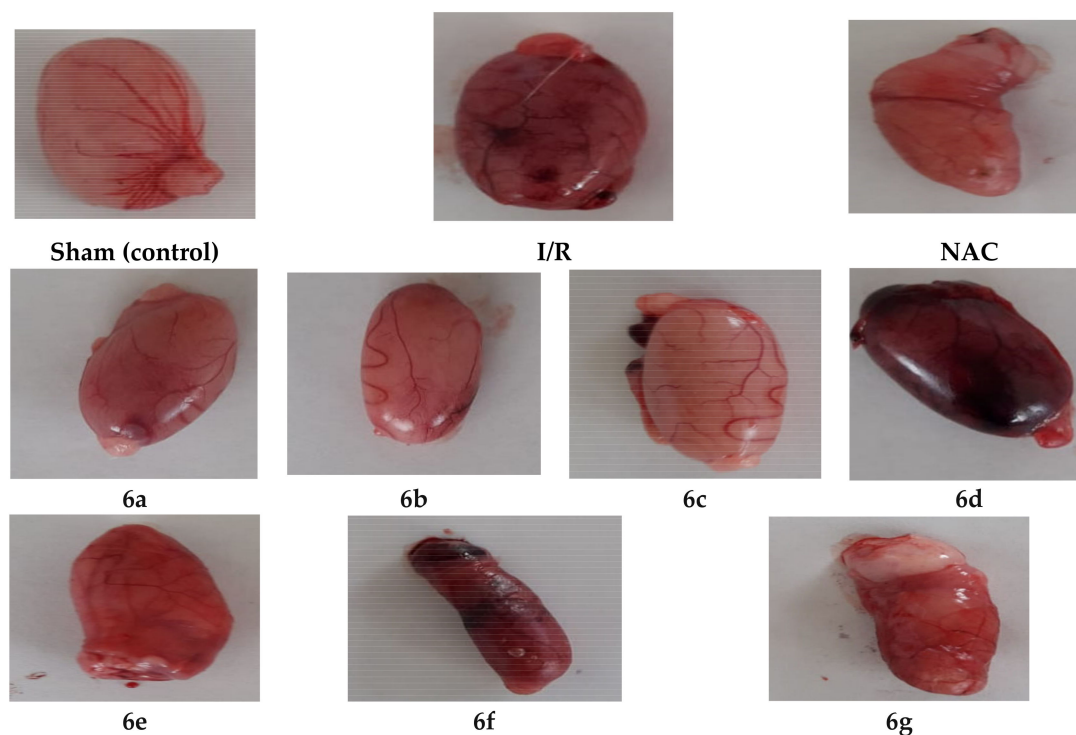


Figure 5. Photos of testicular specimens for groups of sham, I/R, reference (*N*-acetylcysteine, NAC) and treated with compounds **6a–g**.

Table 3. The expression of the biomarkers during apoptosis in testis.

* Biomarker	Effect During Apoptosis in Testis
TNF α [47], MDA [48], Caspase-3 [1]	Increase
TAC [49], Testosterone [50]	Decrease

* TNF = tumor necrosis factor, MDA = malondialdehyde, TAC = total antioxidant capacity.

2.2.1. In Vivo Assay of Antioxidant Biomarkers in Testis (MDA and TAC)

During the long testicular torsion, oxidation damage affects the testis by the production of the reactive oxygen species (ROS) [51]. Excessive generation of the ROS interacts with lipids, proteins, and nucleic acids, which has an adverse effect on cell function and damage [52]. The testis has high cell

metabolism such that excessive ROS production weakens antioxidant capacity [53]. Malondialdehyde (MDA) is the end product of lipid peroxidation and increased MDA level has an adverse effect on sperm fertility [54]. Furthermore, total antioxidant capacity (TAC) is the measure of the number of free radicals scavenged by a test solution, being used to evaluate the antioxidant capacity of biological samples [55]. The data collected in Table S3 (Supplementary Materials) have identified that there was a significant increase in testicular MDA with a significant decrease in testicular TAC in the I/R group as well as compounds **6d** and **6f** when compared to sham control and NAC groups. These findings indicate that both **6d** and **6f** are the worst antiapoptotic compounds amongst all the synthesized compounds. Meanwhile, **6a–c** are the most potent derivatives showing a significant decrease in testicular MDA (conc 62.38, 61.84 and 64.93 nmol/g tissue, respectively) along with a significant increase in testicular TAC (5.48, 4.62, 4.78 mmol/g tissue; respectively) relative to NAC (67.58 nmol/g tissue and 4.45 mmol/g tissue, respectively) when compared to I/R group. Compounds **6e** and **6g** were still showing significantly not improved testicular MDA and TAC (Figure 6A).

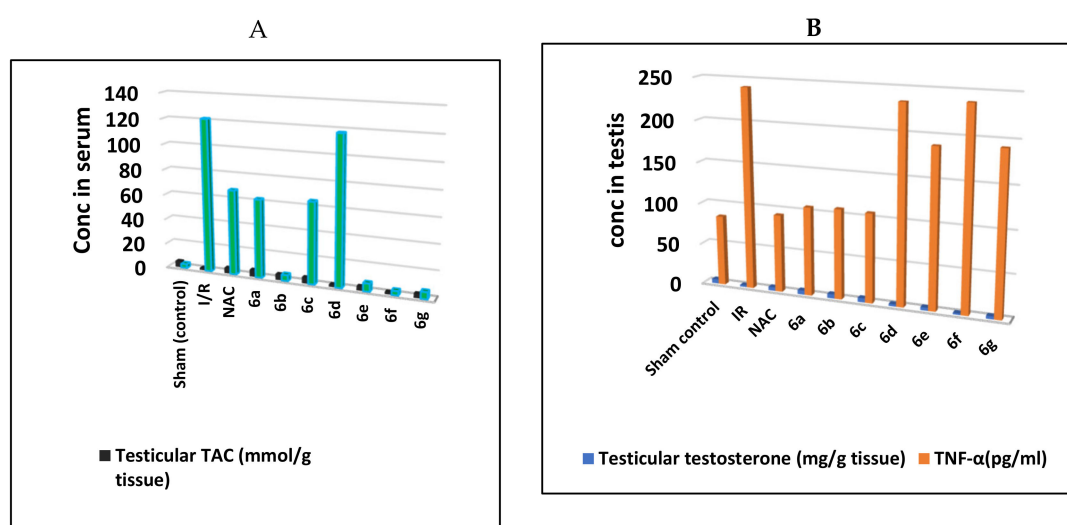


Figure 6. Concentrations of (A); testicular malondialdehyde (MDA) and testicular total antioxidant capacity (TAC), (B); testicular testosterone and TNF α in the testis of I/R rats treated with compounds **6a–g** and NAC.

2.2.2. In Vivo Assay of Apoptotic Biomarkers (Testicular Testosterone and TNF α)

It was reported that excessive apoptosis in the testis could damage the Leydig cells and apparent decline in serum testosterone levels [56]. Furthermore, excessive apoptosis of Leydig cells results in decreased testosterone. The assays of the apoptotic biomarkers (testicular testosterone and TNF α) were done in comparison with the sham and NAC treated group and the results were outlined in Table S4 (Supplementary Materials). Groups of I/R and both compounds **6d** and **6f** showed a significant decrease in testicular testosterone with a significant increase in TNF- α when compared to sham control and NAC groups (Figure 6B). Interestingly, groups of compounds **6a–c** showed a significant increase in testicular testosterone with a significant decrease in TNF- α in comparison to the IR group and relative to the reference NAC group. On the other hand, compounds **6e** and **6g** revealed remarkable testicular testosterone and TNF- α (Table S4 in Supplementary Materials).

2.2.3. Assay of Caspase-3

Assay of Caspase-3 Inhibition in Serum

The above findings indicate a remarkable antiapoptotic activity of our target compounds that inhibition of caspase-3 might probably be the suggested target mechanism. Caspases can delay apoptosis, implicating a potential role in drug screening efforts [1]. Therefore, we studied the mechanism

of the caspase-3 inhibition activity. Caspase-3 was assayed in the serum of rats treated with **6a–g** in comparison with sham and the NAC treated group, as shown in Table S5 (Supplementary Materials). Groups of I/R and both compounds **6d** and **6f** showed significant caspase-3 when compared to sham control and NAC groups (Figure 7). Moreover, groups of compounds **6a–c** showed a significant decrease in caspase-3 in comparison to the IR group and relative to the reference NAC group. On the other hand, compounds **6e** and **6g** displayed a remarkable testicular caspase-3 as in Table S5 (Supplementary Materials).

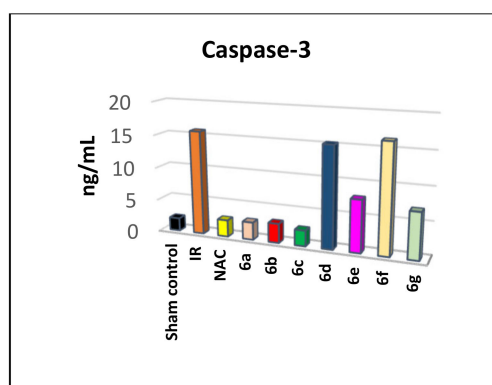


Figure 7. Caspase-3 level (ng/mL) in the serum of testicular I/R rats treated with compounds **6a–g** and NAC.

Caspases-3, 8 and 9 Selectivity Assay in MOLT-4 Cell Line

To outline compounds **6c** antiapoptotic mechanism whether it is through the inhibition of the intrinsic or the extrinsic pathway or both, their effect on caspase-8 and caspase-9 was also evaluated. Moreover, to investigate the caspase-3 inhibition as well as selectivity being the suggested mechanism, the most active caspase-3 inhibitor 1,2,3-triazole/biquinolinone hybrid **6c** was further studied for its effect on caspase-3, 8, and 9 and compared to the reference NAC.

The assay utilizes synthetic peptide substrate DEVD-AFC (AFC, 7-amino-4-trifluoromethyl coumarin). Cell-based caspase-3, and proapoptotic caspase-8 and 9 cleave the synthetic substrate to release free AFC, which can then be quantified by fluorometry. Compounds to be screened can directly be added to the reaction, and the level of inhibition of caspase-3 activity can be determined by comparison of the fluorescence intensity in samples with and without the testing inhibitors. Compound **6c** showed downregulation in the level of active caspase-3 with $IC_{50} = 16.31$ nM compared to NAC ($IC_{50} = 46.83$ nM) as shown in (Table S1, Supplementary Materials). Moreover, the effect of compound **6c** on caspases-8 and 9 was also evaluated revealing a decrease in the levels of caspases 8 and 9 with $IC_{50} = 35.57$ and 96.24 nM, respectively, relative to NAC and compared to the untreated control (Figure 8). The data indicate that **6c** is a putative inhibitor of both intrinsic and extrinsic caspase pathways with more selectivity and potency effect on caspase-3.

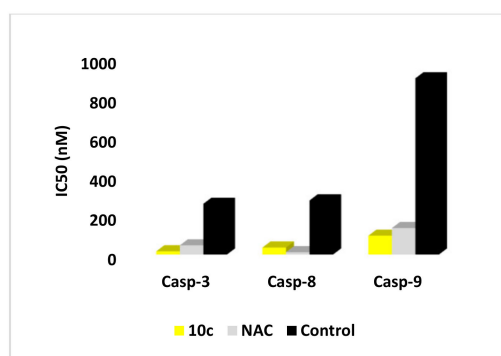


Figure 8. IC_{50} (nM) of compounds **6c** and NAC on the active caspases-3, 8, and 9.

Assay of Cytochrome C in SR Human Cell Line

For more proof of caspase-3 inhibition by our synthesized compounds, cell-based cytochrome C was assayed. It was reported that cytochrome C concentration in the cell has a critical role in the inactivation of caspases and prohibiting the intrinsic apoptosis pathway [57]. Antiapoptotic proteins can inhibit apoptosis by blocking the release of cytochrome C while proapoptotic members function as activators of its release. When cytochrome C level is maintained in mitochondria, caspase-8 and 9 will not be activated leading to caspase-3 inactivation, which in turn ceased apoptosis and reserved the cell from the programmed death [58].

The 1,2,3-triazole/biquinolinone derivative **6c** was evaluated for cytochrome C against the SR human cell line and the results are listed in Table 4. Compound **6c** caused down-expression of cytochrome C level about 3.54 fold, comparable to NAC (4.13 fold), and lower than control. The displayed results could be a good guide for suggesting that antiapoptotic activity may be attributed to the attenuation of cytochrome C and hence inactivation of the intrinsic apoptotic pathway induced by the tested compounds.

Table 4. Effects of compound **6c** and NAC on cytochrome C in SR human cell line.

Code	Cyt C	
	Conc ng/mL	Fold Change
6c	0.28 ± 0.011	3.54
NAC	0.24 ± 0.019	4.13
Control	0.99 ± 0.036	6.03

2.2.4. Histopathological Investigation

Throughout the previous work, results were consistent that motivated us to carry out a histopathological investigation of the tested compounds in the testis.

Spermatogenesis Scoring

The testicular I/R significantly made more histopathological changes (Figure 9A) of the tested compounds if compared to the control group. Also, it decreased spermatogenesis when compared to the control group by using Johnson's scoring system (Figure 9B). Instead of that, groups of compounds **6a–c** showed no significant difference if compared to the reference (NAC) rats. On the other hand, compounds **6e** and **6g** showed weak significant differences if compared to the reference group. Whereas compounds **6d** and **6f** showed a highly significant histopathological difference compared to the reference group (all p -value < 0.005).

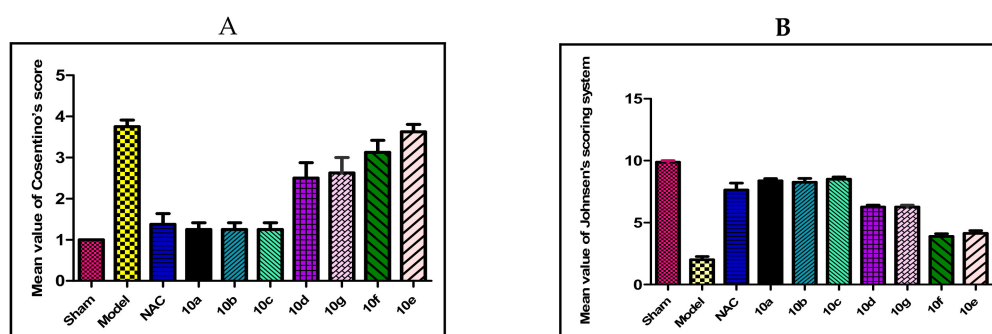


Figure 9. The histopathological findings of (A); Cosentino's score, (B); Johnson's scoring. Results were represented by the mean ± SE ($n = 6$).

Histopathological Study

Hematoxylin and eosin slides of the sham group displayed the normal histological testicular morphology. The seminiferous tubules were seen lined with stratified testicular epithelium rested on basement membranes. The interstitial tissues contained clusters of Leydig cells (Figure 10A), while sections from the I/R group showed distorted seminiferous tubules lined by disorganized epithelium. Ruptured tubules and distorted Leydig cells and sloughed cells could be also observed (Figure 10B). NAC group showed more or less normal seminiferous tubules and Leydig cells except some areas displayed distorted tubules and widening of inter-tubular spaces (Figure 10C). Furthermore, drug 6a–c showed more or less normal seminiferous tubules with germinal epithelium and Leydig cells (Figure 11). Additionally, 6e and 6g showed dilated seminiferous tubules. Distorted Leydig cells with dilated blood vessels (BV) were frequently seen among the sections (Figure 12). Compounds 6d and 6f exhibited ruptured seminiferous tubules with distorted Leydig cells. Dilated blood vessels and the presence of amyloid substance were also found (Figure 13).

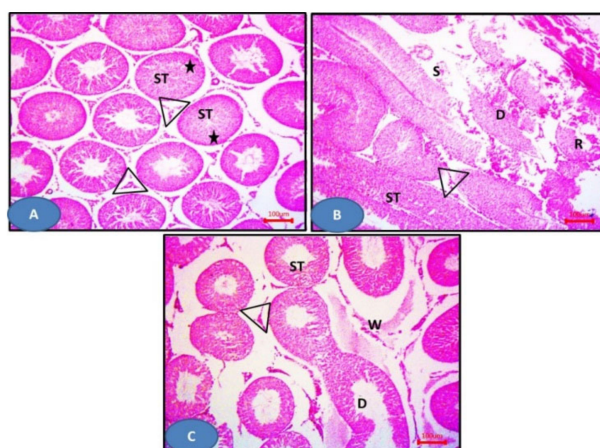


Figure 10. Photomicrographs of sections of the testis: (A) The sham group showing seminiferous tubules (ST) with germinal epithelium (stars) and Leydig cells (triangles). (B) Model group showing distorted seminiferous tubules lined (D) by disorganized epithelium. Notice the ruptured tubules (R) and the distorted Leydig cells (triangles). Sloughed cells (S) can be observed. (C) The NAC group showing more or less normal seminiferous tubules (ST) and Leydig cells (triangles), except some areas showing distorted tubules (ST). Notice the widening of inter-tubular spaces (W). H&E \times 100.

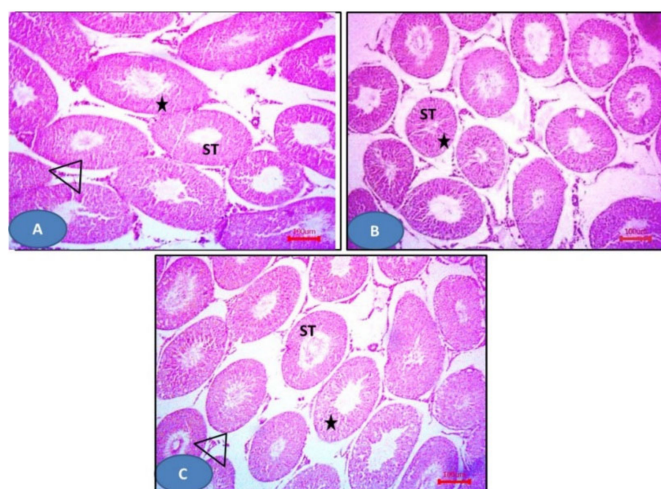


Figure 11. Photomicrographs of sections of the testis: (A–C) 6a–c respectively showing more or less normal seminiferous tubules (ST) with germinal epithelium (stars) and Leydig cells (triangles). H&E \times 100.

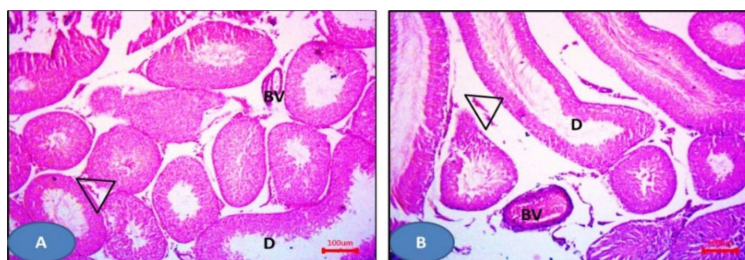


Figure 12. Photomicrographs of sections of the testis: (A,B) **6e** and **6g** respectively showing dilated seminiferous tubules (D) with distorted Leydig cells (triangles). Notice the dilated blood vessels. H&E $\times 100$.

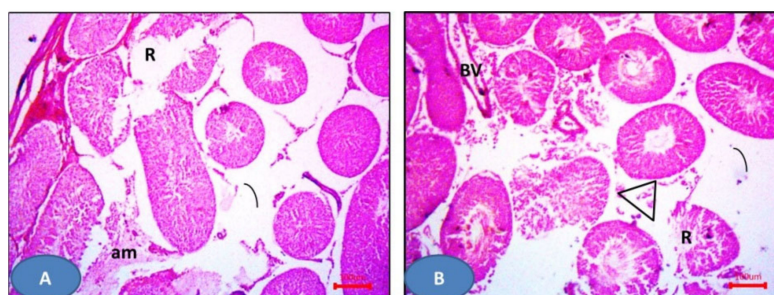


Figure 13. Photomicrographs of sections of the testis: (A,B) **6d** and **6f** respectively showed the ruptured seminiferous tubules (R) with distorted Leydig cells (triangles). Notice the dilated blood vessels (BV) and the amyloid substance (am). H&E $\times 100$.

In summary, testicular I/R induced many histopathological modalities in the form of germinal cell derangement and atrophy with necrosis, which is significantly different from the sham group by Cosentino's score. Additionally, the spermatogenesis process was significantly decreased if compared to the sham control group using Johnson's score, which confirmed the pathological damage in response to testicular I/R. These results match with the previously published reported results [59].

3. Computational Analysis

3.1. Docking Studies

Aiming to investigate the docking fitness scores of the bioactive conformations of the synthesized compounds and their specificity for caspase-3, docking of compounds **6a–g** was performed at the active site of the caspase-3 enzyme in complex with NAC to explore their binding modes as caspase-3 inhibitors using Molecular Operating Environment (MOE[®]) version 2014.09 (Montreal, QC, Canada). The crystal structure of caspase-3 protein taken from the protein data bank (PDB: 3GJQ) was used as a good template for many validation sets of structure-based pharmacophore modeling of caspase-3 inhibitors.

Molecular docking results were found to agree with the findings of biochemical and histopathological studies, for the highly active derivatives such as **6a–c** by caspase-3 inhibition activity.

3.2. Binding Modes of Tested Compounds with Caspase-3 Enzyme Active Site

As a first step, validation of the docking protocol settings was done through the re-docking of the extracted co-crystallized ligand Ac-IEPD-Cho from the 3D structure using the same protocol for the docked compounds (RMSD 0.38 Å). The used docking protocol closely reproduced the bound structure confirming the confidence in our docking study. The docked compounds were built using the builder tool in MOE then subjected to an energy minimization followed by a systematic conformational search using the default force field and settings, then the lowest energy conformer of each molecule was used for the docking experiment.

The docking study will be valid proof of the previously displayed mechanistic antiapoptotic study. Docking will be based on some aspects (i) binding with a caspase-3 catalytic binding site (ASP135 and LYS137), where the more binding, the more caspase inhibitory activity and the more antiapoptotic activity [60] along with the high-affinity binding score (*s*-score). (ii) The value of root-mean-square deviation refinement of atomic positions (RMSD_refine), whereas its values for the tested compounds are of range 1.79–3.68 Å, reflecting the fitting and stability of the compound conformation into the pocket.

Recently, it is reported that an RMSD < 2.0 Å corresponds to good docking solutions. On the other hand, docking solutions with RMSD between 2.0 and 3.0 Å deviate from the position of the reference, but they keep the desired orientation. Finally, docking solutions with RMSD > 3.0 Å are completely wrong [61]. This could be explained by the fact that the highly active compounds **6b** showed low RMSD refined (root mean square deviation refinement) values near to the pose of the co-crystallized ligand, which ensures both the validity of the docking protocol and the good interactions of the ligands and the main residues at the active site domain.

Table S2 (Supplementary Materials) illustrates the binding free energies from the best favorable poses with the least *S*-score of the tested compounds at pKa = 7 and are shown in Figure 14. Most of the tested compounds have high binding affinity to the enzyme as their binding free energy (ΔG) values range from −0.6 to −9.4 Kcal/mol better than the reference NAC ($\Delta G = -0.8$ to −6.5 Kcal/mol).

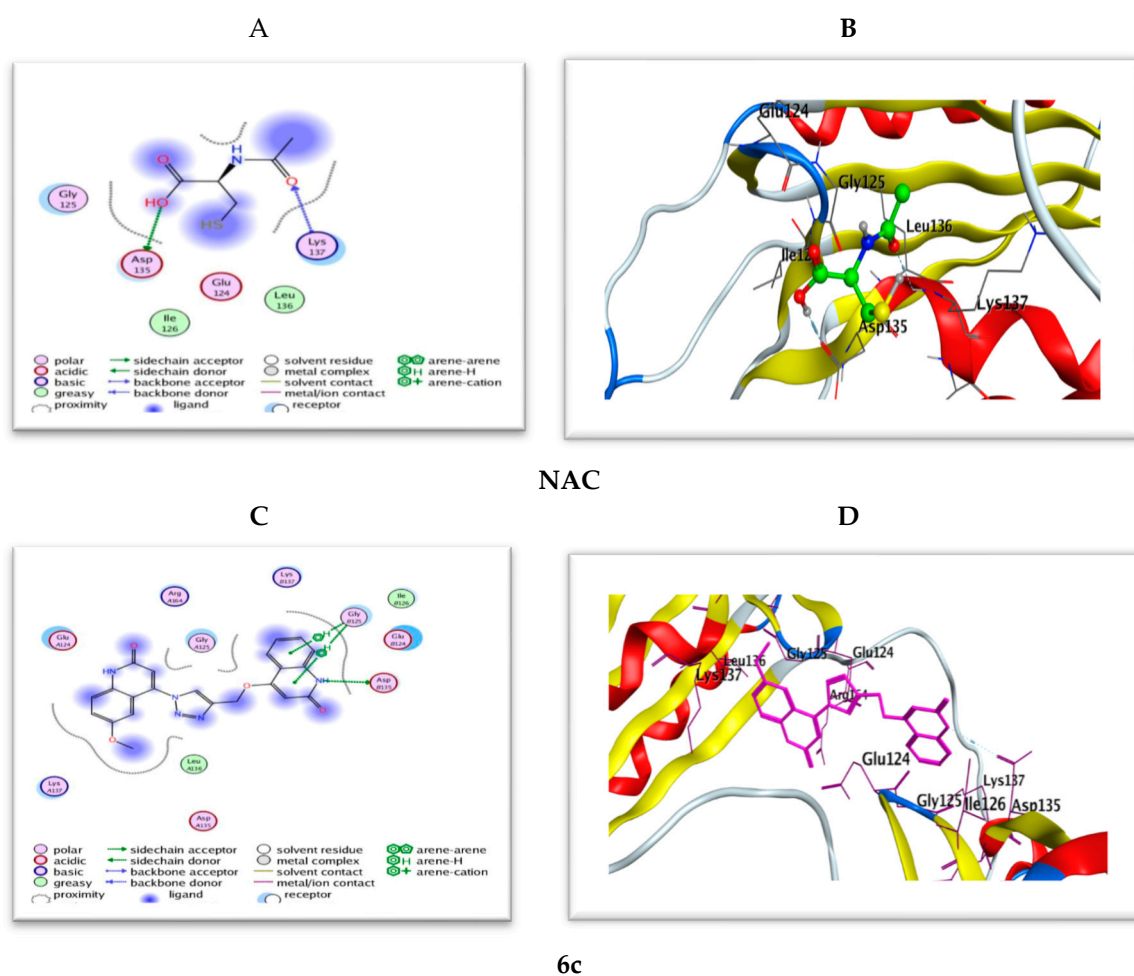


Figure 14. (A,B) 2D and 3D diagrams illustrate the binding modes of the reference NAC and (C,D) are for **6c** interacted with the active site of caspase-3 (PDB: 3GJQ).

The docking study results of bis(quinolinone)/1,2,3-triazole derivatives **6a–g** showed better mode of interactions than the reference NAC. The 2D and 3D diagrams of the compounds showed crucial

binding with LYS137 GLY125 and THR140 through quinoline NH and triazole C=N functionality. The next study, therefore, moves on to discuss the hypothesis that says linking with ASP135 with good binding energy and a low RMSD value give good caspase inhibition. Furthermore, stabilization of the reference NAC within the active site occurred through two strong hydrogen bond interactions with amino acid residues ASP135 and LYS137. Compound **6c** (Figure 14) exhibited the same interactions with the conserved amino acid ASP135 as NAC; however, most of the tested derivatives **6a,b**, and **d-g** possess interaction with LYS137 as the reference.

Most of the compounds showed interaction greater than NAC to interact with the same amino acids with an additional hydrophobic bond with GLY125, THR140, and PHE158. On the other hand, compounds **6f** (Figure S2) dismissed hydrogen binding interactions with the amino acid residue ASP135 and LYS137. Also, compound **6c** kept two hydrogen bond interactions with GLY125.

Furthermore, overall docking results revealed that the most potent new compounds **6a-c**, which are lacking substitutions at position R¹ and R³ of the two quinoline moieties showed binding modes within the active site indicating hydrogen bonding interaction with LYS137 (Figure 15). This finding is in agreement with what is explained in the SAR section that unsubstitution on the two 2-quinolone relieve steric hindrance, which may probably enhance binding with the caspase-3 active site.

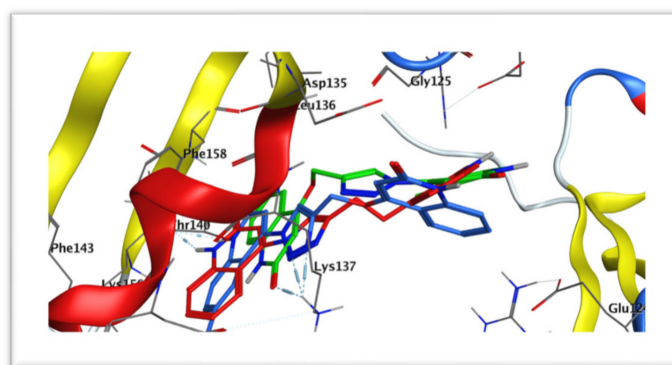


Figure 15. Docking of compounds **6a** (red) aligned with **6b** (blue) and **6c** (green) within the active site of caspase-3 (PDB: 3GJQ).

3.3. Prediction of Physicochemical Properties, Pharmacokinetics, and Drug-Likeness Profile In Silico

In clinical trials, election of a new drug is considered so complicated due to inappropriate ADME (absorption, distribution, metabolism, and excretion) possessions in addition to the costs needed for developing a new drug. Hence, design and applied new drugs are considered to be complicated. Therefore, evaluating the pharmacokinetic properties of a new drug is a critical step in the process of drug development and can directly contribute to optimization efforts into recovered analogs [62]. Currently, The most promising compounds can be picked in silico ADMET screens, reducing the chance of degradation of drugs in late stages [63]. To achieve a desired in vivo response, it should be balanced between pharmacodynamics and pharmacokinetic properties. Also, information about regimen and drug dose is given by the prediction of brain penetration, volume of distribution, oral bioavailability, and clearance. Many parameters such as drug solubility S, partition coefficients, polar surface PSA, cell permeability, human intestinal absorption HIA, and drug-likeness score have been studied during virtual screening methods. An available oral drug elected in agreement with Lipinski's rule if the molecular weight is less than 500, Log P is not higher than five, the number of hydrogen bond acceptors is less than 10 and the number of donor hydrogen bond donors is less than five [64]. The number of rotatable bonds reflects molecular flexibility that plays an important role in oral bioavailability and means less orally active in a flexible molecule. The number of hydrogen bonding groups has also been

suggested as a consideration to substitute for the polar surface area (PSA) and also to measure the percentage absorption (%ABS) as it is inversely proportional to tPSA

$$\%ABS = 109 - 0.345 \text{ tPSA} \quad (1)$$

The higher oral bioavailability exhibited by compounds with tPSA of fewer than 140 Å² and 10 or fewer rotatable bonds.

Herein, we used Pre-ADMET (<https://preadmet.bmdrc.kr/>) [65], Molinspiration (<https://www.molinspiration.com/>) [66], Molsoft (<https://www.molsoft.com/about.html>) [67], and SwissADME (<http://www.swissadme.ch/>) software [62] for predicting the pharmacokinetic parameters of the reported compounds. The results are shown in Table 5, all the target compounds **6a–g** obey the Lipinski's rule with Log P values from 2.32 to 2.73 (<5), an MW range from 385.38 to 415.40 (<500), HBD from 1 to 2 (≤5) and HBA from 5 to 6 (<10). They would theoretically show a strong oral absorption and this property cannot be attributed to variations in their bioactivity. Furthermore, the topological PSA values of the compounds ring are between 94.80 and 114.89 Å² (<140 Å²) and the corresponding percentage oral absorption was between 72.55 and 69.36%, exhibit strong permeability, absorption and transport across a biological membrane. Furthermore, the drug-likeness model score and solubility for compounds was confirmed by Molsoft software (Table 6). Aqueous solubility can change the absorption and distribution characteristics. The more positive the drug-likeness model scores, the more likely it is to be a drug molecule, and these compounds have fulfilled their solution ability specifications at LogS values between −3.30 and −3.78 (above Log S = −4). Positive model-scores (0.45, 0.36 and 0.31 respectively) were anticipated for compounds **6b**, **6c** and **6f** while that for other compounds was negative (−0.18 to −0.23).

Table 5. Physicochemical and lipophilicity of the target compounds using Swiss absorption, distribution, metabolism, and excretion (ADME) and Molinspiration software.

Compound	Physicochemical Properties									
	Lipophilicity Consensus log P	MW ^a g/mol	Heavy Atoms	Aromatic Heavy Atoms	Rot. Bond	H-Bond Acc.	H-Bond Don.	MR ^b	TPSA ^c (Å ²)	%ABS ^d
6a	2.41	385.38	29	25	4	5	2	108.59	105.66	72.55
6b	2.45	399.40	30	25	4	5	1	113.49	94.80	76.29
6c	2.32	415.40	31	25	5	6	1	114.67	104.03	73.11
6d	2.73	399.40	30	25	4	5	2	113.56	105.66	72.55
6e	2.64	399.40	30	25	4	5	2	113.56	105.66	72.55
6f	2.72	413.43	31	25	4	5	1	118.46	94.80	76.29
6g	2.38	415.40	31	25	5	6	2	115.08	114.89	69.36

Abbreviation: MW^a, molecular weight; MR^b, molar refractivity; TPSA^c, topological polar surface area; %ABS^d: percentage of absorption.

Table 6. Lipinski drug-likeness of the target compounds using Molsoft and Swiss ADME software.

Compound	Log S ^a	Drug Likeness Model Score	Lipinski Violations	Bioavailability Score
6a	−3.30	−0.23	0	0.55
6b	−3.48	0.45	0	0.55
6c	−3.53	0.36	0	0.55
6d	−3.60	−0.18	0	0.55
6e	−3.60	−0.18	0	0.55
6f	−3.78	0.31	0	0.55
6g	−3.36	−0.21	0	0.55

Log S^a: Log of solubility.

Additionally, the following pharmacokinetic parameters were experimented with in silico using Pre-ADMET software: blood–brain barrier partition coefficient (BBB), cytochrome inhibition of cytochrome P4502D6 (CYP2D6), Caco2, coefficient (human colon adenocarcinoma), MDCK (Madin–Darby canine kidney cells) permeability coefficient, human intestinal absorption (HIA) and human plasma–protein binding (PPB). The results of the ADME parameters are shown in Table 7. The findings from compounds with moderate CNS absorption ranges between 0.039 and 0.075 (≤ 0.1); investigated compounds exhibited medium to low cell permeability in Caco-2, MDCK models range from 21.79 and 24.63, 4.39 to 1.02 nm/s, respectively. This is aligned with non-inhibitors of the CYP2D6 enzyme and thus may pretend to have no interactions with CYP2D6 inhibitors and/or inducers. Furthermore, all the compounds **6a–g** showed high human intestinal absorption values of 95.58 to 100%, indicating very well-absorbed compounds especially for **6a**, which exhibited 100% intestinal absorption. The examined compounds were found to be highly-bound to human plasma proteins from 89.41 to 97.71% except for **6g** that was low bounded to plasma protein 84.71%.

Table 7. ADME data of tested compounds calculated using preADMET software.

Compound	BBB ^a	Caco-2 ^b	Pharmacokinetics			CYP 2D6 ^f
			HIA ^c	MDCK ^d	PPB ^e	
6a	0.041	22.28	100.00	16.84	90.09	Non
6b	0.069	23.96	96.82	6.56	98.07	Non
6c	0.075	23.23	97.44	6.31	94.65	Non
6d	0.039	21.81	95.58	4.39	89.29	Non
6e	0.039	21.79	95.58	4.39	89.41	Non
6f	0.067	24.63	96.74	1.02	97.71	Non
6g	0.05	21.85	96.01	8.51	84.71	Non

^a **BBB**: blood–brain barrier penetration; ^b **CACO-2**: permeability through cells derived from human colon adenocarcinoma; ^c **HIA**: percentage human intestinal absorption; ^d **MDCK**: permeability through Madin–Darby canine kidney cells; ^e **PPB**: plasma protein binding; ^f **CYP2D6**: cytochrome P450 2D6.

3.4. Structure–Activity Relationship

Based on the previous results, we can deduce that when the two quinoline moieties are unsubstituted at position R¹ and R³ as in compounds **6a–c**, the antiapoptotic activity revealed the highest potency. Meanwhile, upon substitution of R³ with an electron-donating group such as methyl (compound **6e**) or -OCH₃ group (compound **6g**), the antiapoptotic activity was particularly diminished to become abolished upon substitution either at R¹ only (compound **6d**) or at R² and R³ for compound **6f**. These biochemical findings can be explained as a substitution at both two quinoline-2-one rings, which would hinder interaction with the target protein that may be attributed to the resulting steric hindrance. Because the target compounds **6a–g** revealed interesting downregulation of caspase-3 in testis, this work has undergone further histopathological mechanistic investigations to prove exactly the explained hypothesis. The in silico study revealed that all the target compounds **6a–g** obey the Lipinski's rule in addition to the drug-likeness model score and solubility for compounds was confirmed by Molsoft software. The ADME predictions displayed moderate to good parameters for **6a–g**. These results confirm the successful design of the target compounds.

4. Material and Methods

4.1. General Information

All reagents were used as purchased from Merck (St. Louis, MO, USA). The progress of all reactions was monitored with thin-layer chromatography (TLC) on Merck alumina-backed TLC plates and visualized under UV light. Spectra were measured in DMSO-*d*₆ on a Bruker AV-400 spectrometer (400 MHz for ¹H, 100 MHz for ¹³C, and 40.54 MHz for ¹⁵N, in the Chemistry Department, Florida Institute of Technology, 150 W University Blvd, Melbourne, FL 32901, USA. Chemical shifts are

expressed in δ (ppm) versus internal tetramethylsilane (TMS) = 0 ppm for ^1H and ^{13}C , and external liquid ammonia = 0 ppm for ^{15}N . Coupling constants are stated in Hz. Correlations were established using ^1H - ^1H COSY, and ^1H - ^{13}C and ^1H - ^{15}N HSQC and HMBC experiments. All ^{15}N signals were observed indirectly, via HSQC or HMBC experiments. Chemical shifts (δ) are reported in parts per million (ppm) relative to tetramethylsilane (TMS) as internal standard, and the coupling constants (J) are reported in Hertz (Hz). Splitting patterns are denoted as follows: singlet (s), doublet (d), multiplet (m), triplet (t), quartet (q), doublet of doublets (dd), doublet of triplets (dt), triplet of doublets (td), and doublet of quartet (dq). Melting points (mp) were determined with a Stuart melting point instrument in the Chemistry Department, Florida Institute of Technology, 150 W University Blvd, Melbourne, FL, USA, and are expressed in $^\circ\text{C}$ as well as Mass spectra were recorded on a Finnigan Fab 70 eV at Al-Azhar University, Egypt. Elemental analyses were carried out on a Perkin Elmer device at the Microanalytical Institute of Organic Chemistry, Karlsruhe Institute of Technology, Karlsruhe, Germany.

4.2. Starting Materials

All 4-azidoquinolin-2(1H)-ones **4a–d** were prepared according to the literature as 4-azidoquinolin-2(1H)-one (**4a**) [68,69], 4-azido-6-methyl-quinoline-2(1H)-one (**4b**) [47], 4-azido-6-methoxy-quinoline-2(1H)-one (**4c**) [47] and 4-azido-1-methyl-quinoline-2(1H)-one (**4d**) [69], respectively.

4.3. General Procedure for the Formation of Compounds **5a–c**

To a solution of 6-substituted 4-hydroxy-quinolin-2-(1H)-one (4 mmol) in DMF (30 mL) and K_2CO_3 (1.104 g, 8 mmol) was added propargyl bromide (0.944 g, 8 mmol) dropwise at 30–40 $^\circ\text{C}$ with stirring for 5 h and the reaction mixture was mentioned by TLC. Then the reaction mixture was poured into 200 g ice to give a white precipitate, which was filtered off and recrystallized from ethanol to give products **5a–c**.

4-(Prop-2-yn-1-yloxy)quinolin-2(1H)-one (**5a**). White solid, yield: 112 mg, 40%; mp 210–212 $^\circ\text{C}$; ^1H -NMR (DMSO- d_6) δ_{H} 1.44 (s, 1H; H-1), 7.76 (d, $J = 8.0$, 1H; H-5), 7.53 (dd, $J = 7.7$, 7.7, 1H; H-7), 7.30 (d, $J = 8.2$, 1H; H-8), 7.18 (dd, $J = 7.9$, 7.3, 1H; H-6), 5.97 (s, 1H; H-3), 5.01 (d, $J = 2.2$, 2H; H-4c), 3.75 (t, $J = 2.0$, 1H; H-4e). ^1H -NMR (CDCl_3) δ_{H} 11.95 (b, 1H; H-1), 7.95 (d, $J = 8.1$, 1H; H-5), 7.55 (ddd, $J = 7.7$, 7.7, 1.2, 1H; H-7), 7.41 (d, $J = 8.2$, 1H; H-8), 7.24 (dd, $J = 7.2$, 7.2, 1H; H-6), 6.17 (s, 1H; H-3), 4.88 (d, $J = 2.3$, 2H; H-4c), 2.64 (t, $J = 2.3$, 1H; H-4e). ^{13}C -NMR (DMSO- d_6): δ_{C} 162.91 (C-2), 160.91 (C-4), 138.64 (C-8a), 131.04 (C-7), 122.11 (C-5), 121.44 (C-6), 115.22 (C-8), 114.29 (C-4a), 98.13 (C-3), 79.32 (C-4e), 77.89 (C-4d), 56.34 (C-4c). ^{13}C -NMR (CDCl_3): δ_{C} 163.11 (C-4), 138.10 (C-8a), 131.54 (C-7), 122.94 (C-5), 122.64 (C-6), 116.11 (C-8), 115.47 (C-4a), 97.17 (C-3), 77.17 (C-4e), 76.45 (C-4d), 56.55 (C-4c). ^{15}N -NMR (DMSO- d_6): δ_{N} 144.1 (N-1). ^{15}N -NMR: (CDCl_3): δ_{N} 145.3 (N-1). *Anal. Calcd.* for $\text{C}_{12}\text{H}_9\text{NO}_2$: C, 72.35; H, 4.55; N, 7.03. Found: C, 72.44; H, 4.39; N, 6.99.

6-Methyl-4-(prop-2-yn-1-yloxy)quinolin-2(1H)-one (**5b**). White solid, yield: 176 mg, 60%; mp 214–216 $^\circ\text{C}$; ^1H -NMR (DMSO- d_6): δ_{H} 11.37 (b, 1H; NH-1), 7.55 (bs, 1H; H-5), 7.35 (bd, $J = 8.1$, 1H; H-7), 7.20 (d, $J = 8.1$, 1H; H-8), 5.94 (s, 1H; H-3), 4.99 (bd, $J = 1.2$, 2H; H-4b), 3.75 (bt, 1H; H-4d), 2.35 (s, 3H; CH_3). ^{13}C -NMR (DMSO- d_6): δ_{C} 162.79 (C-2), 160.77 (C-4), 136.65 (C-8a), 132.21 (C-7), 130.47 (C-6), 121.55 (C-5), 115.18 (C-8), 114.19 (C-4a), 98.09 (C-3), 79.26 (C-4d), 77.93 (C-4c), 56.27 (-O- CH_2), 20.45 (CH_3). ^{15}N -NMR (DMSO- d_6): δ_{N} 144.1 (NH). *Anal. Calcd.* for $\text{C}_{13}\text{H}_{11}\text{NO}_2$: C, 73.23; H, 5.20; N, 6.57. Found: C, 73.33; H, 5.08; N, 6.68.

6-Methoxy-4-(prop-2-yn-1-yloxy)quinolin-2(1H)-one (**5c**). White solid, yield: 155 mg, 50%; mp 220–222 $^\circ\text{C}$; ^1H -NMR (DMSO- d_6): δ_{H} 11.36 (b, 1H; NH-1), 7.50 (bs, 1H; H-5), 7.35 (bd, $J = 7.8$, 1H; H-7), 7.23 (d, $J = 7.8$, 1H; H-8), 5.91 (s, 1H; H-3), 4.99 (bd, $J = 1.3$, 2H; H-4b), 3.75 (bt, 1H; H-4d), 3.73 (s, 3H; -O- CH_3). ^{13}C -NMR (DMSO- d_6): δ_{C} 162.59 (C-2), 160.76 (C-4), 151.35 (C-6), 135.50 (C-8a), 132.21 (C-7), 122.05 (C-5), 115.48 (C-8), 114.13 (C-4a), 97.99 (C-3), 79.22 (C-4d), 77.93 (C-4c), 55.98 (-O- CH_2), 55.13 (-O- CH_3). ^{15}N -NMR (DMSO- d_6): δ_{N} 144.1 (NH). *Anal. Calcd.* for $\text{C}_{13}\text{H}_{11}\text{NO}_3$: C, 68.11; H, 4.84; N, 6.11. Found: C, 68.29; H, 4.77; N, 5.98.

4.4. General Procedure for the Formation of Compounds 6a–g

In a round bottom flask, mixing (1 mmol) of terminal alkynes **5a–c** in 20 mL dimethylformamide (DMF), CuI (10 mol%) was stirred for 10 min at room temperature. Then, 4-azido compounds **4a–d** (1.0 mmol) were added to the mixture. The reaction mixture was allowed to stir at 50–60 °C for 24 h. The reaction was monitored with TLC. After completion, the reaction mixture was poured on 200 g ice and extracted by filtration.

4-((1-(2-Oxo-1,2-dihydroquinolin-4-yl)-1H-1,2,3-triazol-4-yl)methoxy)quinolin-2(1H)-one (**6a**). Yellowish green solid, yield: 328 mg, 85%; mp 300–302 °C; ¹H-NMR (DMSO-*d*₆): δ_H 12.29 (bs, 1H; NH-1), 11.43 (bs, 1H; NH-1'), 9.00 (s, 1H; H-5''), 7.84 (d, *J* = 7.6, 1H; H-5'), 7.67 (dd, *J* = 7.1, 7.1, 1H; H-7), 7.52–7.48 (m, 3H; H-5,7',8), 7.29–7.27 (m, 2H; H-6,8'), 7.16 (dd, *J* = 7.0, 7.0, 1H; H-6'), 6.91 (s, 1H; H-3), 6.21 (s, 1H; H-3'), 5.47 (s, 2H; -O-CH₂). ¹³C-NMR (DMSO-*d*₆): δ_C 163.12 (C-2'), 161.75 (C-4'), 160.96 (C-2), 143.59 (C-8a), 142.41 (C-4''), 139.45 (C-4), 138.67 (C-8a'), 131.89 (C-7), 131.02 (C-7'), 126.74 (C-5''), 124.02 (C-5), 122.60, 122.50 (C-5',6), 121.32 (C-6'), 117.82 (C-3), 115.93 (C-4a/4a'), 115.15 (C-8), 114.46 (C-4a'/4a), 114.41 (C-8'), 97.93 (C-3'), 61.81 (-O-CH₂). EI-MS (*m/z*, %): 385 (M⁺, 26). *Anal. Calcd for* C₂₁H₁₅N₅O₃: C, 65.45; H, 3.92; N, 18.17. Found: C, 65.60; H, 3.88; N, 18.29.

6-Methyl-4-(((2-oxo-1,2-dihydroquinolin-4-yl)oxy)methyl)-1H-1,2,3-triazol-1-yl)quinolin-2(1H)-one (**6b**). Yellowish green solid, yield: 360 mg, 90%; mp 298 °C; NMR: see Table 2. EI-MS (*m/z*, %): 399 (M⁺, 10). *Anal. Calcd for* C₂₂H₁₇N₅O₃: C, 66.16; H, 4.29; N, 17.53. Found: C, 66.09; H, 4.33; N, 17.69.

6-Methoxy-4-(((2-oxo-1,2-dihydroquinolin-4-yl)oxy)methyl)-1H-1,2,3-triazol-1-yl)-quinolin-2(1H)-one (**6c**). White solid, yield: 270 mg, 65%; mp 295–297 °C; ¹H-NMR (DMSO-*d*₆): δ_H 12.21 (bs, 1H; NH-1), 11.44 (bs, 1H; H-1'), 9.04 (s, 1H; H-5''), 7.84 (d, *J* = 8.0, 1H; H-5'), 7.53 (dd, *J* = 7.5, 7.5, 1H; H-7'), 7.45 (d, *J* = 9.0, 1H; H-8), 7.36 (dd, *J* = 9.0, 2.6, 1H; H-7), 7.30 (d, *J* = 8.1, 1H; H-8'), 7.16 (dd, *J* = 7.4, 7.4, 1H; H-6'), 6.96 (d, *J* = 2.6, 1H; H-5), 6.91 (s, 1H; H-3), 6.21 (s, 1H; H-3'), 5.49 (s, 2H; H-4a'), 3.71 (s, 3H; H-6b). ¹³C-NMR (DMSO-*d*₆): solubility was low. Carbon signals were observed indirectly, using HSQC or HMBC experiments. δ_C 162.1 (C-4'), 154.9 (C-6), 143.4 (C-4), 142.8 (C-4''), 134.9 (C-8a), 131.4 (C-7'), 127.1 (C-5''), 123.0 (C-5'), 121.7 (C-7), 121.5 (C-6'), 118.7 (C-3), 117.9 (C-8), 115.5 (C-8'), 106.2 (C-5), 62.3 (-O-CH₂), 55.8 (OCH₃). C-2, 2', 3', 4a, 4a', and 8a' were not observed. EI-MS (*m/z*, %): 415 (M⁺, 30). *Anal. Calcd for* C₂₂H₁₇N₅O₄: C, 63.61; H, 4.12; N, 16.86. Found: C, 63.72; H, 4.29; N, 16.99.

1-Methyl-4-(((2-oxo-1,2-dihydroquinolin-4-yl)oxy)methyl)-1H-1,2,3-triazol-1-yl)quinolin-2(1H)-one (**6d**). White solid, yield: 270 mg, 68%; mp 285–287 °C; ¹H-NMR (DMSO-*d*₆): δ_H 11.43 (bs, 1H; NH-1'), 8.99 (s, 1H; H-5''), 7.84 (d, *J* = 8.0, 1H; H-5'), 7.80 (dd, *J* = 7.8, 7.8, 1H; H-7), 7.74 (d, *J* = 8.4, 1H; H-8), 7.52 (dd, *J* = 8.0, 8.0, 1H; H-7'), 7.51 (d, *J* = 8.1 Hz; 1H, H-5), 7.36 (dd, *J* = 7.5, 7.5, 1H; H-6), 7.30 (d, *J* = 8.2, 1H; H-8'), 7.16 (dd, *J* = 7.8, 7.8, 1H; H-6'), 7.04 (s, 1H; H-3), 6.22 (s, 1H; H-3'), 5.48 (s, 2H; -O-CH₂), 3.74 (s, 3H; N-CH₃). ¹³C-NMR (DMSO-*d*₆): δ_C 163.12 (C-2'), 161.75 (C-4'), 160.30 (C-2), 142.59 (C-4), 142.41 (C-4''), 140.15 (C-8a), 138.67 (C-8a'), 132.33 (C-7), 131.02 (C-7'), 126.96 (C-5''), 124.50 (C-5), 122.75 (C-6), 122.49 (C-5'), 121.32 (C-6'), 117.30 (C-3), 115.57, 115.54 (C-4a, 8), 115.15 (C-8'), 114.41 (C-4a'), 97.93 (C-3'), 61.79 (-O-CH₂), 29.59 (CH₃). ¹⁵N-NMR (DMSO-*d*₆): δ_N 247.0 (N-1''), 147.2 (N-1), 144.1 (N-1'). EI-MS (*m/z*, %): 399 (M⁺, 20). *Anal. Calcd for* C₂₂H₁₇N₅O₃: C, 66.16; H, 4.29; N, 17.53. Found: C, 65.99; H, 4.36; N, 17.49.

6-Methyl-4-(((1-(2-oxo-1,2-dihydroquinolin-4-yl)-1H-1,2,3-triazol-4-yl)methoxy)quinolin-2(1H)-one (**6e**). Yellowish green, yield: 320 mg, 80%; mp 272–274 °C; ¹H-NMR (DMSO-*d*₆): δ_H 12.29 (bs, 1H; NH-1), 11.35 (bs, 1H; NH-1'); 8.99 (s, 1H; H-5''), 7.67 (dd, *J* = 7.6, 7.6, 1H; H-7), 7.61 (bs, 1H; H-5'), 7.51 (d, *J* = 9.1, 1H; H-5), 7.49 (d, *J* = 9.2, 1H; H-8), 7.35 (d, *J* = 8.2, 1H; H-7'), 7.27 (dd, *J* = 7.6, 7.6, 1H; H-6), 7.21 (d, *J* = 8.2, 1H; H-8'), 6.91 (s, 1H; H-3), 6.19 (s, 1H; H-3'), 5.46 (s, 2H; -O-CH₂), 2.33 (s, 3H; H-6a'). ¹³C-NMR (DMSO-*d*₆): δ_C 163.01 (C-2'), 161.62 (C-4'), 160.97 (C-2), 143.61 (C-4), 142.36 (C-4''), 139.45 (C-8a), 136.68 (C-8a'), 132.21 (C-7'), 131.90 (C-7), 130.38 (C-6'), 126.81 (C-5''), 124.03 (C-5), 122.61 (C-6), 121.81 (C-5'), 117.84 (C-3), 115.94 (C-8), 115.13 (C-8'), 114.47 (C-4a), 114.29 (C-4a'), 97.90 (C-3'), 61.68 (-O-CH₂), 20.45 (CH₃). ¹⁵N-NMR (DMSO-*d*₆) δ_N 247.8 (N-1''), 152.2 (N-1), 143.2 (N-1'). EI-MS (*m/z*, %): 399 (M⁺, 22). *Anal. Calcd for* C₂₂H₁₇N₅O₃: C, 66.16; H, 4.29; N, 17.53. Found: C, 66.09; H, 4.44; N, 17.38.

6-Methyl-4-((1-(6-methyl-2-oxo-1,2-dihydroquinolin-4-yl)-1H-1,2,3-triazol-4-yl)methoxy)quinolin-2(1H)-one (**6f**). White solid, yield: 363 mg, 88%; mp 270–272 °C; $^1\text{H-NMR}$ (DMSO- d_6): δ_{H} 12.22 (bs, 1H; NH-1), 11.36 (bs, 1H; NH-1'), 8.98 (s, 1H; H-5''), 7.61 (bs, 1H; H-5'), 7.49 (d, $J = 8.0$, 1H; H-7), 7.39 (d, $J = 8.0$, 1H; H-8), 7.34 (d, $J = 8.1$, 1H; H-7'), 7.26 (bs, 1H; H-5), 7.20 (d, $J = 8.1$, 1H; H-8'), 6.87 (s, 1H; H-3), 6.19 (s, 1H; H-3'), 5.46 (s, 2H; -O-CH₂), 2.32 (s, 3H; H-6a'), 2.31 (s, 3H; H-6a). $^{13}\text{C-NMR}$ (DMSO- d_6): δ_{C} 163.04 (C-2'), 161.61 (C-4'), 160.83 (C-2), 143.41 (C-4), 142.36 (C-4''), 137.53 (C-8a), 136.69 (C-8a'), 133.19 (C-7), 132.19 (C-7'), 131.79 (C-6), 130.37 (C-6'), 126.81 (C-5''), 123.14 (C-5), 121.81 (C-5'), 117.87 (C-3), 115.92 (C-8), 115.14 (C-8'), 114.40, 114.31 (C-4a', 4a), 97.91 (C-3'), 61.71 (-O-CH₂), 20.52 (C-6a), 20.45 (C-6a'). $^{15}\text{N-NMR}$ (DMSO- d_6): δ_{N} 248.0 (N-1''), 151.5 (N-1), 143.2 (N-1'). EI-MS (m/z , %): 413 (M^+ , 10). *Anal. Calcd for* C₂₃H₁₉N₅O₃: C, 66.82; H, 4.63; N, 16.94. Found: C, 66.98; H, 4.77; N, 16.99.

6-Methoxy-4-((1-(2-oxo-1,2-dihydroquinolin-4-yl)-1H-1,2,3-triazol-4-yl)methoxy)quinolin-2(1H)-one (**6g**). Pale yellow, yield: 270 mg, 65%; mp 300–302 °C; $^1\text{H-NMR}$ (DMSO- d_6) δ_{H} 12.29 (bs, 1H; NH-1), 11.33 (bs, 1H; NH-1'), 8.99 (s, 1H; H-5''), 7.66 (dd, $J = 7.3, 7.3$, 1H; H-7), 7.49 (m; 2H, H-5, 8), 7.26 (m; 3H, H-6, 5', 8'), 7.21 (m; 1H, H-7'), 6.90 (s; 1H, H-3), 6.22 (s, 1H; H-3'), 5.49 (s; 2H, -O-CH₂), 3.77 (s, 3H; -OCH₃). $^{13}\text{C-NMR}$ (DMSO- d_6): δ_{C} 162.67 (C-2'), 161.26 (C-4'), 160.95 (C-2), 153.97 (C-6'), 143.60 (C-4), 142.41 (C-4''), 139.45 (C-8a), 133.18 (C-8a'), 131.89 (C-7), 126.76 (C-5''), 123.98 (C-5), 122.58 (C-6), 119.90 (C-7'), 117.86 (C-3), 116.62 (C-8'), 115.94 (C-8), 114.82, 114.48 (C-4a, 4a'), 104.33 (C-5'), 98.41 (C-3'), 61.79 (-O-CH₂), 55.51 (-OCH₃). $^{15}\text{N-NMR}$ (DMSO- d_6): δ_{N} 247.9 (N-1''), 142.7 (N-1). EI-MS (m/z , %): 415 (M^+ , 60). *Anal. Calcd for* C₂₂H₁₇N₅O₄: C, 63.61; H, 4.12; N, 16.86. Found: C, 63.77; H, 4.10; N, 17.00.

5. Biochemical Assay

5.1. Assay of Antioxidant Biomarkers in Testis (MDA and TAC)

TAC was assessed by the colorimetric technique using commercial kits (El-Minia, Egypt) (See Supplementary Materials). Testicular MDA, an index of lipid peroxidation, was determined by using 1,1,3,3-tetramethoxypropane as standard [70] (See Supplementary Materials).

5.2. Assay of Apoptotic Biomarkers (Testicular Testosterone, TNF- α , and Caspase-3)

TNF- α was measured by ELISA kit (Elabscience, Houston, TX, USA). Caspase-3 was measured by ELISA kit Cusabio, Houston, TX, USA (See Supplementary Materials). Testosterone concentration in testicular samples was determined by the ELISA kit ("DRG", Marburg, Germany) (See Supplementary Materials).

5.3. Assay of Caspases

5.3.1. Assay of Caspase-3, 8, and 9 Inhibition

The Caspase-3 Inhibitor Drug Screening Kit (Catalog #JM-K153-100; 15 B Constitution Way Woburn, MA 01801, USA) provides an effective means for screening caspase inhibitors using fluorometric methods. The assay utilizes synthetic peptide substrate DEVD-AFC (AFC, 7-amino-4-trifluoromethylcoumarin). Active caspase-3 cleaves the synthetic substrate to release free AFC, which can then be quantified by fluorometry. Compounds to be screened can directly be added to the reaction and the level of inhibition of caspase-3 activity can be determined by comparison of the fluorescence intensity in samples with and without the testing inhibitors. (See Supplementary Materials).

5.3.2. Assay of Cytochrome C

Cells were collected from American Type Culture Collection to be grown in SR containing 10% fetal bovine serum at 37 °C, stimulated with the compounds to be tested for cytochrome C using Cytochrome C Human ELISA Kit (ab119521—Cytochrome C Human ELISA Kit, Vaccera institute, Egypt) [57] (See Supplementary Materials).

5.4. Histopathological Investigation

Multiple testicular specimens were stained by hematoxylin-eosin (ab245880, Abcam, Cambridge, MA, USA) using Cosentino's score [59] for semi-quantitation of pathological changes in different seminiferous tubules. By using Johnson's scoring system [59], the effect of ischemia on the spermatogenesis can be studied (See Supporting Materials).

5.4.1. Photography

An Olympus light microscopy and digital camera (Olympus, Markham, ON, Canada), were used in this study. Images were executed using Adobe Photoshop.

5.4.2. Morphometric Study

Semi-quantitative data were measured and counted per section in ten randomly selected non-overlapping fields using power $\times 400$ magnifications of the sections from each rat [71]. The results were carried out using the Image J program analysis software (Image J 1.48V, Maryland, MD, USA; Wayne Rasb and National Institutes of Health).

5.4.3. Statistical Analysis

Data were evaluated as means (standard error of the mean). One-way analysis of variance (ANOVA) with the use of Turkey's post-test was carried out for the analysis of the results to detect the significant difference statistically. p values < 0.05 were considered significant.

5.5. Computational Analysis

5.5.1. Molecular Docking Study

The docking simulation study was carried out using Molecular Operating Environment (MOE[®]) version 2014.09, Chemical Computing Group Inc., Montreal, QC, Canada). The computational software operated under "Windows XP" installed on an Intel Pentium IV PC with a 1.6 GHz processor and 512 MB memory. The target compounds were constructed into a 3D model using the builder interface of the MOE program and docked into the active site of caspase-3 (PDB: 3GJQ). Checking their structures and the formal charges on atoms by 2D depiction was carried out and the energy, was minimized until an RMSD (root mean square deviations) gradient of 0.01 Kcal/mol and RMS (Root Mean Square) distance of 0.1 Å with MMFF94X (Merck molecular force field 94x) force-field and the partial charges were automatically calculated (See Supplementary Materials).

5.5.2. Prediction of Physicochemical Properties, Pharmacokinetics, and Drug-Likeness Profile In Silico

The physicochemical and lipophilicity of the target compounds were collected using Swiss ADME software (<http://www.swissadme.ch/index.php>) and Molinspiration software (<https://preadmet.bmdrc.kr/>). In addition, Lipinski drug-likeness of the target compounds were obtained by using Molsoft software (<https://www.molsoft.com/>) and Swiss ADME software. The percent of absorption was calculated through this equation:

$$\%ABS = 109 - 0.345 \text{ tPSA} \quad (2)$$

where TPSA: topological polar surface area; %ABS: percentage of absorption.

5.6. Ethical Approval

Minia University Faculty of Medicine, Research Ethics Committee "BFMREC" approved this research proposal regarding the source of the animals, health status, inclusion criteria, exclusion criteria,

caging, comfort, and the detailed experimental design and procedures. It was conducted in agreement with the NIH Guide for Care and Use of Laboratory Animals. The approval number is: 251-2/2018.

6. Conclusions

A series of biquinoline-2-one/1,2,3-triazole hybrids **6a–g** have been synthesized and identified with different spectroscopic techniques. The antiapoptotic activity of the target compounds in the testis was biochemically evaluated compared with the reference NAC. The most robust compounds were **6a–c**, revealing promising antiapoptotic and antioxidant readings. Moreover, they exhibited a caspase-3 inhibition level of about 2.66, 2.94, and 2.39 ng/mL, respectively. Compound **6c** can be evaluated as a hit for further screenings to acquire more active antiapoptotic agents due to its selectivity toward caspase-3 rather than caspase-8 and -9 as well as a higher cytochrome C potency with conc 0.28 ng/mL. Further histopathological study was performed in a specimen of testis treated with the tested compounds. Furthermore, the molecular docking study was performed on the caspase-3 active site revealing a good interaction with the enzyme. Finally, a computational prediction of physicochemical properties, pharmacokinetics, and drug-likeness profile in silico revealed that compound **6a–c** should be taken into consideration as good antiapoptotic candidates for further study.

Supplementary Materials: The following are available online, Figure S1: 2D and 3D diagrams illustrate the binding modes of the reference NAC and **6a–g** interacted with the active site of caspase-3 (PDB: 3GJQ), Table S1: Effect of compounds **6c** and NAC on the active Cell-based caspases-3, 8 and 9 in MOLT-4 cell line, Table S2: Energy scores for the complexes formed by the tested compounds **6a–g** and the reference NAC in the active site of caspase-3 (PDB: 3GJQ), Table S3: Testicular MDA and Testicular TAC concentrations in testis of I/R rats treated with compounds **6a–g** and NAC, Table S4: Testicular testosterone and TNF α concentrations in testis of I/R rats treated with compounds **6a–g** and NAC, Table S5: Caspase-3 level in serum of testicular I/R rats treated with compounds **6a–g** and NAC.

Author Contributions: E.M.E.-S.: conceptualization; methodology, writing; A.A.A.: conceptualization, writing, revising and submission; M.B.A.: writing, revising; A.B.B.: NMR, revision; S.M.N.A.-H.: histology, revision; W.Y.A.: pharmacology and revision; S.B.: revision; E.M.N.A.: biology, writing and revision. All authors have read and agreed to the published version of the manuscript.

Funding: This research received no external funding.

Acknowledgments: The authors thank the Deanship of Scientific Research at Prince Sattam Bin Abdulaziz University under the research project No. 10302/1/2019. Also, we acknowledge support by the KIT-Publication Fund of the Karlsruhe Institute of Technology. The NMR spectrometer at Florida Institute of Technology was purchased with assistance from the U.S. National Science Foundation (CHE 03-42251).

Conflicts of Interest: The authors declare no conflict of interest. The authors declare that they have no known competing interests.

References

1. Aly, A.A.; Sayed, S.M.; Abdelhafez, E.-S.M.; Abdelhafez, S.M.N.; Abdelzaher, W.Y.; Raslan, M.A.; Ahmed, A.E.; Thabet, K.; El-Reedy, A.A.; Brown, A.B. New quinoline-2-one/pyrazole derivatives; design, synthesis, molecular docking, anti-apoptotic evaluation, and caspase-3 inhibition assay. *Bioorg. Chem.* **2020**, *94*, 103348. [[CrossRef](#)] [[PubMed](#)]
2. Bulut, S.; Özdemir, B.H. Apoptosis and expression of caspase-3 in cyclosporin-induced gingival overgrowth. *J. Periodontol.* **2007**, *78*, 2364–2368. [[CrossRef](#)] [[PubMed](#)]
3. Sagulenko, V.; Lawlor, K.E.; Vince, J.E. New insights into the regulation of innate immunity by caspase-8. *Arthritis Res. Ther.* **2016**, *18*, 4. [[CrossRef](#)] [[PubMed](#)]
4. Norbury, C.J.; Hickson, I.D. Cellular responses to DNA damage. *Annu. Rev. Pharmacol. Toxicol.* **2001**, *41*, 367–401. [[CrossRef](#)] [[PubMed](#)]
5. Pu, X.; Storr, S.J.; Zhang, Y.; Rakha, E.A.; Green, A.R.; Ellis, I.O.; Martin, S.G. Caspase-3 and caspase-8 expression in breast cancer: Caspase-3 is associated with survival. *Apoptosis* **2017**, *22*, 357–368. [[CrossRef](#)] [[PubMed](#)]

6. Wang, C.-C.; Li, H.; Zhang, M.; Li, X.-L.; Yue, L.-T.; Zhang, P.; Zhao, Y.; Wang, S.; Duan, R.-N.; Li, Y.-B. Caspase-1 inhibitor ameliorates experimental autoimmune myasthenia gravis by innate dendritic cell IL-1-IL-17 pathway. *J. Neuroinflammation* **2015**, *12*, 118. [[CrossRef](#)] [[PubMed](#)]
7. Akpan, N.E. The Intrinsic Caspase Death Pathway in Stroke Neurodegeneration. Ph.D. Thesis, Columbia University, New York, NY, USA, 2013.
8. Wang, X.-J.; Cao, Q.; Zhang, Y.; Su, X.-D. Activation and regulation of caspase-6 and its role in neurodegenerative diseases. *Annu. Rev. Pharmacol. Toxicol.* **2015**, *55*, 553–572. [[CrossRef](#)]
9. Singh, P.K.; Kumar, A. Mitochondria mediates caspase-dependent and independent retinal cell death in *Staphylococcus aureus* endophthalmitis. *Cell Death Discov.* **2016**, *2*, 1–11. [[CrossRef](#)]
10. Sun, C.; Liu, H.; Guo, J.; Yu, Y.; Yang, D.; He, F.; Du, Z. MicroRNA-98 negatively regulates myocardial infarction-induced apoptosis by down-regulating Fas and caspase-3. *Sci. Rep.* **2017**, *7*, 1–11. [[CrossRef](#)]
11. Woolbright, B.L.; Ding, W.-X.; Jaeschke, H. *Caspase Inhibitors for the Treatment of Liver Disease: Friend or Foe?* Taylor & Francis: Abingdon-on-Thames, UK, 2017.
12. Malysheva, I.; Topchieva, L.; Barysheva, O.; Kurbatova, I.; Vasykova, O.; Vezikova, N.; Marusenko, I.; Nemova, N. The level of cytokines and expression of caspase genes in rheumatoid arthritis. *Dokl. Biochem. Biophys.* **2016**, *468*, 226–228. [[CrossRef](#)]
13. Aziz, M.; Jacob, A.; Wang, P. Revisiting caspases in sepsis. *Cell Death Dis.* **2014**, *5*, 1526–1532. [[CrossRef](#)] [[PubMed](#)]
14. Hwang, H.S.; Kim, H.A. Chondrocyte apoptosis in the pathogenesis of osteoarthritis. *Int. J. Mol. Sci.* **2015**, *16*, 26035–26054. [[CrossRef](#)]
15. Qi, X.; Gurung, P.; Malireddi, R.S.; Karmaus, P.W.; Sharma, D.; Vogel, P.; Chi, H.; Green, D.R.; Kanneganti, T.-D. Critical role of caspase-8-mediated IL-1 signaling in promoting Th2 responses during asthma pathogenesis. *Mucosal. Immunol.* **2017**, *10*, 128–138. [[CrossRef](#)]
16. Slee, E.A.; Adrain, C.; Martin, S.J. Executioner caspase-3,-6, and-7 perform distinct, non-redundant roles during the demolition phase of apoptosis. *J. Biol. Chem.* **2001**, *276*, 7320–7326. [[CrossRef](#)] [[PubMed](#)]
17. Walsh, J.G.; Cullen, S.P.; Sheridan, C.; Lüthi, A.U.; Gerner, C.; Martin, S.J. Executioner caspase-3 and caspase-7 are functionally distinct proteases. *Proc. Natl. Acad. Sci. USA* **2008**, *105*, 12815–12819. [[CrossRef](#)] [[PubMed](#)]
18. Dokmeci, D. Testicular torsion, oxidative stress and the role of antioxidant therapy. *Folia Med.* **2006**, *48*, 16–21.
19. Taati, M.; Moghadasi, M.; Dezfoulian, O.; Asadian, P. Effects of ghrelin on testicular ischemia/reperfusion-induced injury. *Acta Med. Iran.* **2016**, *54*, 32–38.
20. Wilhelm Filho, D.; Torres, M.A.; Bordin, A.L.; Crezcynski-Pasa, T.B.; Boveris, A. Spermatic cord torsion, reactive oxygen and nitrogen species and ischemia-reperfusion injury. *Mol. Asp. Med.* **2004**, *25*, 199–210. [[CrossRef](#)]
21. Al-Maghrebi, M.; Kehinde, E.O.; Anim, J.T. Long term testicular ischemia-reperfusion injury-induced apoptosis: Involvement of survivin down-regulation. *Biochem. Biophys. Res. Commun.* **2010**, *395*, 342–347. [[CrossRef](#)]
22. Karaguzel, E.; Kadihasanoglu, M.; Kutlu, O. Mechanisms of testicular torsion and potential protective agents. *Nat. Rev. Urol.* **2014**, *11*, 391–399. [[CrossRef](#)]
23. Özdemir, S.B. Synthesis of novel fluoroquinolone-triazole hybrid compounds as antimicrobial agents. *J. Turk. Chem. Soc. Sect. A Chem.* **2016**, *3*, 515–534. [[CrossRef](#)]
24. Michael, J.P. Quinoline, quinazoline and acridone alkaloids. *Nat. Prod. Rep.* **2002**, *19*, 742–760. [[CrossRef](#)]
25. Paeshuysse, J.; Vliegen, I.; Coelmont, L.; Leyssen, P.; Tabarrini, O.; Herdewijn, P.; Mittendorfer, H.; Easmon, J.; Cecchetti, V.; Bartenschlager, R. Comparative in vitro anti-hepatitis C virus activities of a selected series of polymerase, protease, and helicase inhibitors. *Antimicrob. Agents Chemother.* **2008**, *52*, 3433–3437. [[CrossRef](#)]
26. Elbastawesy, M.A.; Ramadan, M.; El-Shaier, Y.A.; Aly, A.A.; Abuo-Rahma, G.E.-D.A. Arylidenes of Quinolin-2-one scaffold as Erlotinib analogues with activities against leukemia through inhibition of EGFR TK/STAT-3 pathways. *Bioorg. Chem.* **2020**, *96*, 103628. [[CrossRef](#)] [[PubMed](#)]
27. Pastrana-Gómez, C.A.; Almonacid-Urrego, C.C.; Velasco-Montejo, B.E.; Mendieta-Zerón, H.; Cuevas-Yáñez, E. Antimycotic sensitivity evaluation against *Candida* ATCC species of 1,2,3-triazoles derived from 5-chloro-2-(2,4-dichlorophenoxy) phenol. *Med. Chem. Res.* **2020**, *29*, 417–425. [[CrossRef](#)]

28. Sanghvi, Y.S.; Bhattacharya, B.K.; Kini, G.D.; Matsumoto, S.S.; Larson, S.B.; Jolley, W.B.; Robins, R.K.; Revankar, G.R. Growth inhibition and induction of cellular differentiation of human myeloid leukemia cells in culture by carbamoyl congeners of ribavirin. *J. Med. Chem.* **1990**, *33*, 336–344. [[CrossRef](#)]
29. Bascal, Z.; Holden-Dye, L.; Willis, R.; Smith, S.; Walker, R. Novel azole derivatives are antagonists at the inhibitory GABA receptor on the somatic muscle cells of the parasitic nematode *Ascaris suum*. *Parasitology* **1996**, *112*, 253–259. [[CrossRef](#)]
30. Allali, M.; Benjelloun, G.T.; Chahboun, N.; Mouacha, Y.; Bennani, L.; Ouahidi, I.; Ibjibijen, J.; Nassiri, L. Synthesis, characterization and the antibacterial activity of a new [1,2,3]triazole derivative. *J. Mater. Environ. Sci.* **2017**, *8*, 2916–2920.
31. Hou, J.; Liu, X.; Shen, J.; Zhao, G.; Wang, P.G. The impact of click chemistry in medicinal chemistry. *Expert Opin. Drug Discov.* **2012**, *7*, 489–501. [[CrossRef](#)]
32. Kojima, M.; Iwakiri, R.; Wu, B.; Fujise, T.; Watanabe, K.; Lin, T.; Amemori, S.; Sakata, H.; Shimoda, R.; Oguzu, T.; et al. Effects of antioxidative agents on apoptosis induced by ischaemia-reperfusion in rat intestinal mucosa. *Aliment. Pharmacol. Ther.* **2003**, *18*, 139–145. [[CrossRef](#)]
33. Kim, Y.-R.; Oh, S.-K.; Lee, T.; Lee, I.-K.; Lee, K.-Y.; Kim, U.-K. Protective effects of 1,2,3-triazole derivative KPR-A020 against cisplatin-induced ototoxicity in murine cochlear cultures. *Int. J. Pediatr. Otorhinolaryngol.* **2017**, *96*, 59–64. [[CrossRef](#)]
34. Park, C.W.; Lee, T.-K.; Cho, J.H.; Kim, I.H.; Lee, J.-C.; Shin, B.-N.; Ahn, J.H.; Kim, S.K.; Shin, M.C.; Ohk, T.G. Rufinamide pretreatment attenuates ischemia-reperfusion injury in the gerbil hippocampus. *Neurol. Res.* **2017**, *39*, 941–952. [[CrossRef](#)] [[PubMed](#)]
35. El-Sheref, E.M.; Aly, A.A.; Ameen, M.A.; Brown, A.B. Synthesis of new 4-(1,2,3-triazolo)quinolin-2(1H)-ones via Cu-catalyzed [3+ 2]cycloaddition. *Monatshfte. Chem.* **2019**, *150*, 747–756. [[CrossRef](#)]
36. Findeisen, M.; Berger, S. *50 and More Essential NMR Experiments: A Detailed Guide*; John Wiley & Sons: Hoboken, NJ, USA, 2013.
37. Steinschifter, W.; Stadlbauer, W. Regioselective Azidation of 2,4-Dichloroquinolines. *J. Prakt. Chem. Chem. Ztg.* **1994**, *336*, 311–318. [[CrossRef](#)]
38. Warsinger, D.M.; Chakraborty, S.; Tow, E.W.; Plumlee, M.H.; Bellona, C.; Loutatidou, S.; Karimi, L.; Mikelonis, A.M.; Achilli, A.; Ghassemi, A. A review of polymeric membranes and processes for potable water reuse. *Prog. Polym. Sci.* **2018**, *81*, 209–237. [[CrossRef](#)] [[PubMed](#)]
39. Stadlbauer, W. Methoden zur Darstellung von 4-Azido-2(1H)-chinolonen. *Monatshfte Chem.* **1986**, *117*, 1305–1323. [[CrossRef](#)]
40. Bräse, S.; Gil, C.; Knepper, K.; Zimmermann, V. Organic azides. An exploding diversity of a unique class of compounds. *Angew. Chem. Int. Ed.* **2005**, *44*, 5188–5240. [[CrossRef](#)]
41. Koelmel, D.K.; Jung, N.; Braese, S. Azides—Diazonium ions—Triazenes: Versatile nitrogen-rich functional groups. *Aust. J. Chem.* **2014**, *67*, 328–336. [[CrossRef](#)]
42. Aly, A.A.; Hassan, A.A.; Mohamed, A.H.; Osman, S.M.; Bräse, S.; Nieger, M.; Ibrahim, M.A.; Mostafa, S.M. Synthesis of 3,3'-methylenebis(4-hydroxyquinolin-2(1H)-ones) of prospective anti-COVID-19 drugs. *Mol. Divers.* **2020**. [[CrossRef](#)]
43. Huisgen, R. 1, 3-dipolar cycloadditions. Past and future. *Angew. Chem. Int. Ed.* **1963**, *2*, 565–598. [[CrossRef](#)]
44. Brahmabhatt, K.G.; Ahmed, N.; Sabde, S.; Mitra, D.; Singh, I.P.; Bhutani, K.K. Synthesis and evaluation of β -carboline derivatives as inhibitors of human immunodeficiency virus. *Bioorg. Med. Chem. Lett.* **2010**, *18*, 2872–2879. [[CrossRef](#)] [[PubMed](#)]
45. D'Amico, F.; Vitale, A.; Piovan, D.; Bertacco, A.; Morales, R.R.; Frigo, A.C.; Bassi, D.; Bonsignore, P.; Gringeri, E.; Valmasoni, M.; et al. Use of N-acetylcysteine during liver procurement: A prospective randomized controlled study. *Liver Transplant.* **2013**, *19*, 135–144. [[CrossRef](#)] [[PubMed](#)]
46. Zhang, F.-X.; Chen, M.; Yang, B.; Chen, H.-W.; Ju, W.-Z.; Wang, J.; Cao, K. The anti-apoptotic effects of N-acetylcysteine in neonatal rat cardiomyocytes underwent hypoxia-reoxygenation injury. *Zhonghua Xin Xue Guan Bing Za Zhi* **2010**, *38*, 445–449.
47. Derin, D.; Soyuncu, H.O.; Guney, N.; Tas, F.; Camlica, H.; Duranyildiz, D.; Yasasever, V.; Topuz, E. Serum levels of apoptosis biomarkers, survivin and TNF-alpha in nonsmall cell lung cancer. *Lung Cancer* **2008**, *59*, 240–245. [[CrossRef](#)] [[PubMed](#)]

48. El-Badry, A.A.-M. Serum Malondialdehyde Levels as a Biomarker of Cellular Injury In Human Fascioliasis. *J. Taibah Univ. Med Sci.* **2006**, *1*, 57–64. [CrossRef]
49. Gökçe, A.; Oktar, S.; Koc, A.; Gonenci, R.; Yalcinkaya, F.; Yonden, Z.; Duru, M. Protective effect of thymoquinone in experimental testicular torsion. *Urol. Int.* **2010**, *85*, 461–465. [CrossRef]
50. Turner, T.T.; Bang, H.J.; Lysiak, J.J. Experimental testicular torsion: Reperfusion blood flow and subsequent testicular venous plasma testosterone concentrations. *Urology* **2005**, *65*, 390–394. [CrossRef]
51. Asghari, A.; Akbari, G.; Meghdadi, A.; Mortazavi, P. Effects of melatonin and metformin co-administration on testicular ischemia/reperfusion injury in rats. *J. Pediatr. Urol.* **2016**, *12*, 410–417. [CrossRef]
52. Yuluğ, E.; Türedi, S.; Alver, A.; Türedi, S.; Kahraman, C. Effects of resveratrol on methotrexate-induced testicular damage in rats. *Sci. World J.* **2013**, *2013*, 1–6. [CrossRef]
53. Motamedi, S.; Asghari, A.; Jahandideh, A.; Abedi, G.; Mortazavi, P. Effects of Echinacea Purpureae Extract on Testicular Ischemia/Reperfusion (I/R) Injury in Rat. *Iran. J. Vet. Med.* **2019**, *13*, 303–313.
54. Ghalehkandi, J.G. Garlic (*Allium sativum*) juice protects from semen oxidative stress in male rats exposed to chromium chloride. *Anim. Reprod.* **2018**, *11*, 526–532.
55. Rubio, C.P.; Hernández-Ruiz, J.; Martínez-Subiela, S.; Tvarijonaviciute, A.; Ceron, J.J. Spectrophotometric assays for total antioxidant capacity (TAC) in dog serum: An update. *BMC Vet. Res.* **2016**, *12*, 166. [CrossRef]
56. Luo, D.-Y.; Yang, G.; Liu, J.-J.; Yang, Y.-R.; Dong, Q. Effects of varicocele on testosterone, apoptosis and expression of StAR mRNA in rat Leydig cells. *Asian J. Androl.* **2011**, *13*, 287–291. [CrossRef] [PubMed]
57. Abdelbaset, M.S.; Abdel-Aziz, M.; Abu-Rahma, G.E.D.A.; Abdelrahman, M.H.; Ramadan, M.; Youssif, B.G. Novel quinoline derivatives carrying nitrones/oximes nitric oxide donors: Design, synthesis, antiproliferative and caspase-3 activation activities. *Arch. Pharm.* **2019**, *352*, 1800270. [CrossRef]
58. Giaccia, A.J.; Kastan, M.B. The complexity of p53 modulation: Emerging patterns from divergent signals. *Genes Dev.* **1998**, *12*, 2973–2983. [CrossRef] [PubMed]
59. Abdel-Aziz, A.M.; Hafez, S.M.N.A. Sitagliptin protects male albino rats with testicular ischaemia/reperfusion damage: Modulation of VCAM-1 and VEGF-A. *Andrologia* **2019**, *52*, e13472. [CrossRef] [PubMed]
60. Sulpizi, M.; Rothlisberger, U.; Carloni, P. Molecular dynamics studies of caspase-3. *Biophys. J.* **2003**, *84*, 2207–2215. [CrossRef]
61. Ramírez, D.; Caballero, J. Is it reliable to take the molecular docking top scoring position as the best solution without considering available structural data? *Molecules* **2018**, *23*, 1038. [CrossRef]
62. Daina, A.; Michielin, O.; Zoete, V. SwissADME: A free web tool to evaluate pharmacokinetics, drug-likeness and medicinal chemistry friendliness of small molecules. *Sci. Rep.* **2017**, *7*, 42717. [CrossRef]
63. Van De Waterbeemd, H.; Gifford, E. ADMET in silico modelling: Towards prediction paradise? *Nat. Rev. Drug Discov.* **2003**, *2*, 192–204. [CrossRef]
64. Rajanarendar, E.; Krishna, S.R.; Nagaraju, D.; Reddy, K.G.; Kishore, B.; Reddy, Y. Environmentally benign synthesis, molecular properties prediction and anti-inflammatory activity of novel isoxazolo[5,4-d]isoxazol-3-yl-aryl-methanones via vinylogous Henry nitroaldol adducts as synthons. *Bioorganic Med. Chem. Lett.* **2015**, *25*, 1630–1634. [CrossRef] [PubMed]
65. Lagorce, D.; Reynes, C.; Camproux, A.C.; Miteva, M.A.; Sperandio, O.; Villoutreix, B.O. In Silico ADME/Tox Predictions. In *ADMET for Medicinal Chemists: A Practical Guide*; John Wiley & Sons: Hoboken, NJ, USA, 2011; pp. 29–124.
66. Cheminformatics, M. Bratislava, Slovak Republic. 2014. Available online: <https://www.molinspiration.com/> (accessed on 1 October 2020).
67. Molsoft, L. Drug-Likeness and Molecular Property Prediction. Available online: <https://www.molsoft.com/about.html> (accessed on 1 October 2020).
68. Steinschifter, W.; Fiala, W.; Stadlbauer, W. Synthesis of oxazolo[4,5-c]quinolones by thermolytic degradation of 4-azido-2(1H)-quinolones. *J. Heterocycl. Chem.* **1994**, *31*, 1647–1652. [CrossRef]
69. Stadlbauer, W.; Laschober, R.; Kappe, T. Potential non-steroidal estrogens and antiestrogens, IV Organic azides in heterocyclic synthesis, part 13: Synthesis of aza- and diazacoumestrols via azido derivatives. *Monatshfte Chem.* **1991**, *122*, 853–861. [CrossRef]

70. Buege, J.A.; Aust, S.D. Microsomal lipid peroxidation. In *Methods in Enzymology*; Academic Press: Cambridge, MA, USA, 1978; Volume 52, pp. 302–310.
71. Hafez, S.M.N.A. Age related changes in the dermal mast cells and the associated changes in the dermal collagen and cells: A histological and electron microscopy study. *Acta Histochem.* **2019**, *121*, 619–627. [[CrossRef](#)] [[PubMed](#)]

Sample Availability: Samples of the compounds are not available from the authors.

Publisher's Note: MDPI stays neutral with regard to jurisdictional claims in published maps and institutional affiliations.



© 2020 by the authors. Licensee MDPI, Basel, Switzerland. This article is an open access article distributed under the terms and conditions of the Creative Commons Attribution (CC BY) license (<http://creativecommons.org/licenses/by/4.0/>).